Student Johannes G. Holten

Shear wave velocity testing in sands

Litterature study

Trondheim, December 2016

PROJECT THESIS: TBA4510
Main supervisor: Professor Steinar Nordal
Co-supervisor: Dr. Jean-Sebastien L'heureux

Department of Civil and Transport Engineering
Norwegian University of Science and Technology (NTNU)

NTNU – Trondheim
Norwegian University of
Science and Technology

Preface

This study is performed as a Project thesis in geotechnics at NTNU in the course TBA4510 as part of the MSc in Civil and Environmental Engineering. It was written during the autumn semester 2016.

Main supervisors of the study has been prof. Steinar Nordal at NTNU and Dr. Jean-Sebastien L'heureux at NGI.

The aim of this study has been to investigate aspects of geodynamics regarding shear wave velocity and the related stiffness parameter small-strain stiffness. During the study field investigations of this parameter there has been performed at a test-site connected to the National Geo-Test Site project in Norway, in addition to laboratory tests for soil classification. Description of field methods and empirical correlations to dynamic properties are presented in the study. In the last part of the study simple preliminary calculations on the measured values from the field investigations is performed.

Trondheim, 2016-12-20

Johannes Gaspar Holten

Summary and Conclusions

This study concerns the propagation of waves in soil, and more specifically the shear wave velocity of sand. The shear wave velocity is a dynamic parameter highly dependent upon variables such as void ratio, confining pressure and strain amplitude in the material. Research has shown that the shear wave velocity can be estimated through empirical CPT-relations.

In this study several field investigations has been performed, such as CPTU, SDMT and MASW for a test site at Øysand, Norway. Soil classification tests has also been performed.

The study concludes that the proposed correlations used to estimate the shear wave velocity seem to perform quite adequately for the Øysand test-site, but that the sample size is too small to make a statistical significant evaluation of the correlations on the basis of the gathered data.

For further work the author recommends that there should be perform more seismic investigations on the Øysand site. These investigations should be complimented with a site-specific correlation for the Øysand site based on regression analysis.

Contents

Chapter 1

Introduction

1.1 Background

Shear wave velocity and the related parameter small-strain stiffness are important geotechnical parameters with applications for many different fields. Especially in problems regarding settlements of foundations the small-strain stiffness is an important tool for dimensioning, and may prevent overly conservative estimates. However, it is still often neglected in geotechnical analyses today, with an exception for some numerical soil models. Within the subject of earthquakes these dynamic properties are also important to account for.

The study is written in conjunction with the National Geo-Test Sites project, led by NGI in cooperation with NTNU, UNIS, SINTEF and the Norwegian Public Roads Administration (NPRA). The primary objective of this project is to establish five national Geo-Test Sites for testing and verifying of new methods for soil investigation. This study is written specifically with the sand test-site at Øysand in mind. So far SDMT, CPTU and MASW test has been performed at the site. The author will also perform laboratory investigation on the soil classification of samples from the site.

1.1.1 Problem Formulation

This study is written as an introductory study of topics connected to shear wave propagation and testing in sand. The main focus lies on the establishing of a theoretical foundation for further work on the master thesis. The study aims to perform preliminary field investigations at the Øysand site, perform basic laboratory classifications from the site and to evaluate some proposed empirical correlations.

1.2 Objectives

The main objectives of this project are

1. Formulate the theoretical background for the subject
2. Identify relevant field methods suitable for the Øysand test-site
3. Get an overview of correlations between shear wave velocity and other gotechnical parameters
4. Perform some preliminary calculations on field tests performed at Øysand
5. Perform laboratory tests for classification of soil from Øysand

1.3 Limitations

The aim of this study has been to investigate theory connected to shear wave velocity. Other forms of wave propagation in soils has therefore, for the most part, been neglected. The study makes no attempt to give a complete mathematical foundation for shear wave propagation, but presents basic differential equations and their solutions.

Methods for estimating shear wave velocity in laboratory is only briefly discussed, and is for the most part not discussed in the study.

The use of dynamic parameters for geotechnical engineering is discussed to some degree, but no in-depth investigations of geotechnical applications are made.

1.4 Structure of the Report

The rest of the report is structured as follows. Chapter 2 gives an introduction to the theory of geodynamics and small-strain stiffness. Chapter 3 presents different methods for field investigation of shear wave velocity. Chapter 4 presents the Øysand test-site and gives an introductory review of the soil distribution. In chapter 5 different empirical correlations are presented. In chapter 6 results from field investigations and predictive values of shear wave velocity is presented. Chapter 7 is a summary and conclusion of the study.

Chapter 2

Theory

This chapter is dedicated to theoretical aspects of wave propagation and small-strain stiffness. Factors affecting important dynamic parameters will be discussed, and the theoretical foundation for wave propagation in soils will be introduced. Theoretical geodynamics will be discussed on the basis of basic mechanical terms, and is greatly influenced by "Geotechnical earthquake engineering" by Kramer (1996). Details of the derivation of equations and relations is in some cases neglected for simplicities case. Theory regarding small-strain stiffness is greatly influenced by "Small-Strain Stiffness of Soils and its Numerical Consequences" by Benz (2007).

2.1 Geodynamics

Wave propagation concerns the oscillation of matter in a material. For the case of geodynamics this material is soils. The oscillation of matter results in a transfer of energy through the wave path. The energy transferred through waves can travel far within a material, whilst the displacement of the individual parts of the matter is limited within a solid (Blackstock, 2000).

The propagation of waves in soils is an important subject for estimating the dynamic response of foundations and vibrations in the soil. Dynamics in soil must be treated through continuum mechanics, even though soils can be highly inhomogeneous and difficult to represent exactly.

There are many different kinds of waves produced by seismic activity in soil. The two main categories of waves are surface waves and body waves. This division is based on whether the wave propagates along the surface of the medium or through the body. We further divide body waves into p- and s-waves, and surface waves into Rayleigh- and Love-waves (Kramer, 1996). In this chapter the focus will be on body-waves.

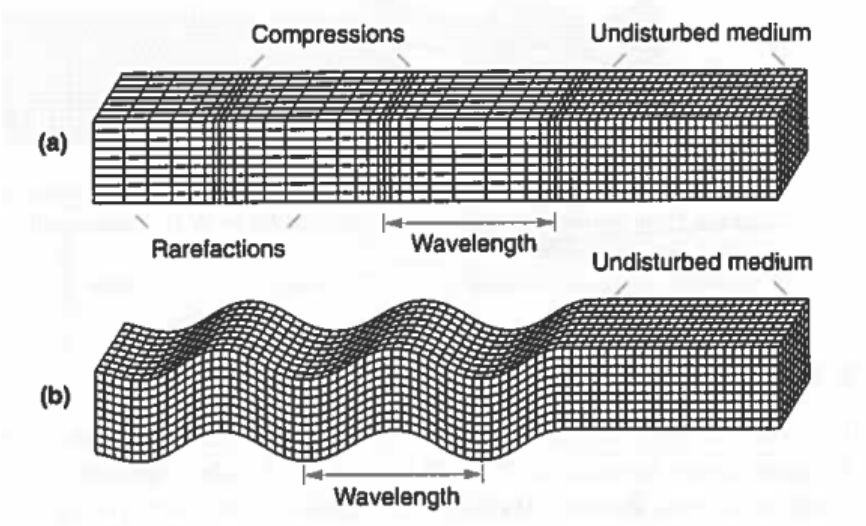

Figure 2.1: Deformation produced by a) p-waves and b) s-waves. Figure taken from (Kramer, 1996).

2.1.1 Wave propagation

For this section an infinite, elastic soil body is assumed. We also assume isotropic material behaviour and a homogeneous material. Wave propagation can, by the definitions made in section 2.1, be descirbed as three-dimensional dispersion of seismic energy. Considering an infinitesimal soil element in a stress state where all sides are exposed to normal and shear stress. Figure 2.2 defines a Cartesian coordinate system with the forces acting upon the soil element. Requiring moment equilibrium we reduce the number of unknowns:

$$\sigma_{xy} = \sigma_{yx}, \quad \sigma_{yz} = \sigma_{zy}, \quad \sigma_{zx} = \sigma_{xz} \tag{2.1}$$

We are then left with the six independent stress components: σ_{xx}, σ_{yy}, σ_{zz}, σ_{xy}, σ_{yz} and σ_{zx}. We then require force equilibrium to obtain the differential equations for the soil element. In this force equilibrium the inertia forces, i.e. the acceleration dependent forces, is included since we want the dynamic force equilibrium. We are then left with the following differential equations (Kramer, 1996):

$$\rho \frac{\partial^2 u}{\partial t^2} = \frac{\partial \sigma_{xx}}{\partial x} + \frac{\partial \sigma_{xy}}{\partial y} + \frac{\partial \sigma_{xz}}{\partial z} \tag{2.2}$$

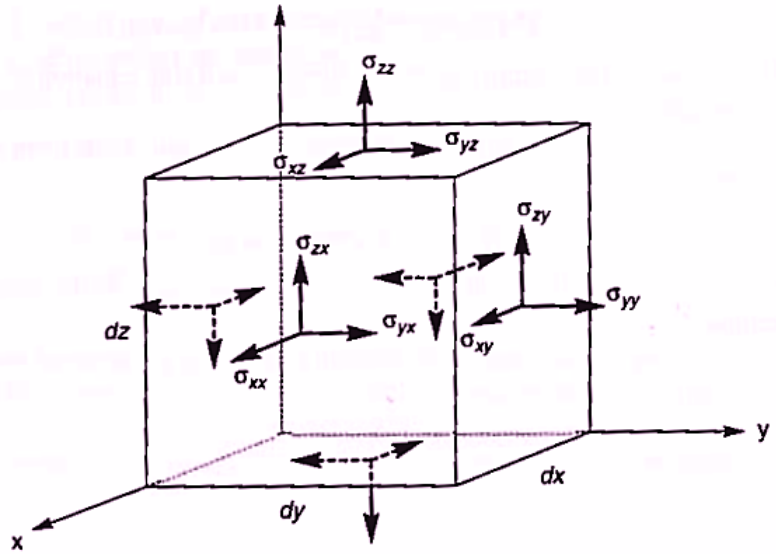

Figure 2.2: Stress notation for infinitesimal 3D element(Kramer, 1996).

$$\rho \frac{\partial^2 v}{\partial t^2} = \frac{\partial \sigma_{yx}}{\partial x} + \frac{\partial \sigma_{yy}}{\partial y} + \frac{\partial \sigma_{yz}}{\partial z} \tag{2.3}$$

$$\rho \frac{\partial^2 w}{\partial t^2} = \frac{\partial \sigma_{zx}}{\partial x} + \frac{\partial \sigma_{zy}}{\partial y} + \frac{\partial \sigma_{zz}}{\partial z} \tag{2.4}$$

By introducing Hooke's law for a three dimensional material with isotropic material properties and rewriting the equations, we get:

$$\rho \frac{\partial^2 u}{\partial t^2} = (\lambda + G) \frac{\partial \tilde{\epsilon}}{\partial x} + G \nabla^2 u \tag{2.5}$$

$$\rho \frac{\partial^2 v}{\partial t^2} = (\lambda + G) \frac{\partial \tilde{\epsilon}}{\partial y} + G \nabla^2 v \tag{2.6}$$

$$\rho \frac{\partial^2 w}{\partial t^2} = (\lambda + G) \frac{\partial \tilde{\epsilon}}{\partial z} + G \nabla^2 w \tag{2.7}$$

where $\tilde{\epsilon}$ is the volumetric strain, and λ and G is alternative material parameters called Lamé's constants defined as:

$$\lambda = \frac{\nu E}{(1+\lambda)(1-2\nu)} \tag{2.8}$$

$$G = \frac{E}{2(1+\nu)} \tag{2.9}$$

P-waves

P-waves are defined as waves that cause volumetric displacement of matter. This implies that p-waves involve no shearing or rotation of the medium (see

figure 2.1 (a)). Another important trait of the p-wave is that the motion of the particles has the same direction as the wave (Kramer, 1996). To obtain the differential equations for the p-wave, also called dilatational wave, one must therefore consider only the volumetric part of the wave. Solving the differential equations for the waves speed yields the following:

$$v_p = \sqrt{\frac{\lambda + 2G}{\rho}} \tag{2.10}$$

The resulting solution is the p-wave velocity, i.e. the velocity in which a p-wave will travel through a elastic medium with isotropic material properties.

S-waves

S-waves, or shear waves, are waves that cause shape deformation, or shearing, as they travel through the medium (Kramer, 1996). A fundamental property of this wave is its equivoluminal or distortional capacity, i.e. the propagation of the wave has no impact on the volume of the material, and all deformation is related to change in shape. The wave is characterized by the fact that the motion of all individual particles is perpendicular to the wave direction (see illustration in figure 2.1 (b)). Due to this particular motion it is natural to speak of two different kinds of shear waves, namely the horizontal and the vertical shear wave. In a horizontal shear wave all particle motion is in the horizontal plane, and opposite for vertical shear waves.

Knowing that shear waves only produce change of shape we want a solution of the differential equation where the change in volume is equal to zero. The resulting solution is the shear wave velocity, i.e. the velocity in which a shear wave will travel through a elastic medium with isotropic material properties. The shear wave velocity is:

$$v_s = \sqrt{\frac{G}{\rho}} \tag{2.11}$$

As we can see the wave speed depends on the shear modulus (stiffness related to shearing) and the material density.

2.1.2 Discussion of assumptions

Considering waves in an elastic material we make the assumptions of a homogenous material, and constant material parameters. Under idealized conditions one would assume that waves may travel indefinitely with no change

in amplitude. In reality we know that this isn't the case, and that amplitudes decrease along the travel path until they completely vanish. Mathematically this reduction of the amplitude can be assigned to two forms of damping in the soil, i.e. material damping and geometrical damping, and the refraction of waves (Kramer, 1996). All these effects can be mathematically accounted for, but this will not be done in this section as this is outside the scope of this paper. Instead a simple description of each will be given for the basic understanding of each phenomena.

Material damping is the conversion of elastic energy of a wave to heat energy. This effect can be accounted for by making a division of the material resistance into an elastic and a viscous part. With viscous damping the specific energy (elastic energy per unit volume) of the material decreases along the path of a traveling wave.

Geometrical damping, also called radiation damping, depicts a decrease in the specific energy due to geometrical spread of a wave. This makes intuitively sense when visualizing a wave originating from a single point. If assumed that the wave propagates as a sphere the "surface area" of the wave increases with the distance from the origin. Even with no material damping it's evident that the energy resulting from the origin will have to spread among this surface, and therefore the specific energy and the amplitude will decrease.

The assumption of a homogenous material is also problematic. Soil as a material is often, if not always, best described as a layered body, with many parts of different stiffness and material behaviour, and where the different layers have varied thickness and extent. Considering the case of a wave traveling through material 1 with given density and material parameters, and then moving into material 2 with different density and material properties (see figure 2.3). When moving into material 2 a refraction of the wave will occur, resulting in a transmitted wave into material 2 and a reflected wave into material 1, due to the difference in characteristics. If material 2 is "stiffer" than material 1, the amplitude of the transmitted wave will be greater than the amplitude of the incident wave, and vice-versa. It should be noted that the refraction of the wave also will depend on the angle in which the wave approaches the boundary between material 1 and 2 (Kramer, 1996).

This sections shows how complex a field geodynamics is and the many challenges connected to accurately predicting seismic dispersion in soils. However, even though the formulations made in this chapter only represent mathematical models, experience show that they can be pretty good at approximating results, and very useful in practice.

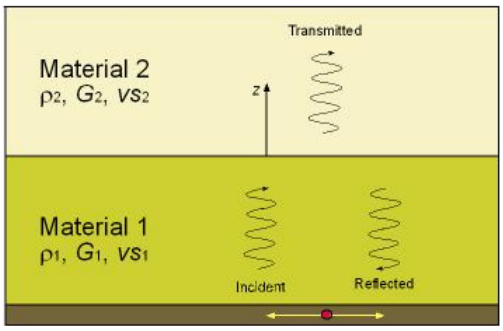

Figure 2.3: Refraction of wave due to layering (Arduino, 2000).

2.2 Small-strain stiffness

Small-strain stiffness, often depicted as G_{max} or G_0, is the shear stiffness the range in *"which soils exhibit almost fully recoverable behaviour"* (Benz, 2007). The strains in this range is very small, which is intuitive since soils are not know to be elastic in behaviour. The small strain range is defined to be $\gamma_s \leq 10^{-5}$ (Benz et al., 2009). The value of the stiffness in this range can be hard to measure properly since the strains are so small. Conventional soil testing methods, e.g. triaxial or oedometer tests, cannot reliably measure the small-strain stiffness, as the minimum value of strain that is measurable with these methods is $\gamma_s \approx 10^{-3}$ (Benz, 2007). Other methods has to be used to measure G_{max}.

In many contexts dynamic stiffness is used as a synonym to small-strain stiffness. Intuitively this seems strange since the dynamic stiffness should account for effects from the strain rate and the inertia forces, while the small-strain stiffness should describe quasi-static conditions. However experiments show that the effect from inertia forces only slightly increases the stiffness in the range of very small strain, and that the two stiffness can be used interchangeably (Stokoe et al., 1999). This also means that dynamic methods can be used to measure the stiffness for small strains. Figure 2.4 shows the variation in the shear modulus, normalized on the small-strain stiffness. The figure also illustrates the methods of measurement that can be used for different ranges of strain.

In geotechnical practice small-strain stiffness is still not widely implemented as a dimensioning parameter, except in some soil models such as the HS-small model (Hardening soil model with small-strain extension). Benz et al. (2009) argues however that it should be more used. One of the arguments is that not accounting for it can result in overestimating settlements and deformation.

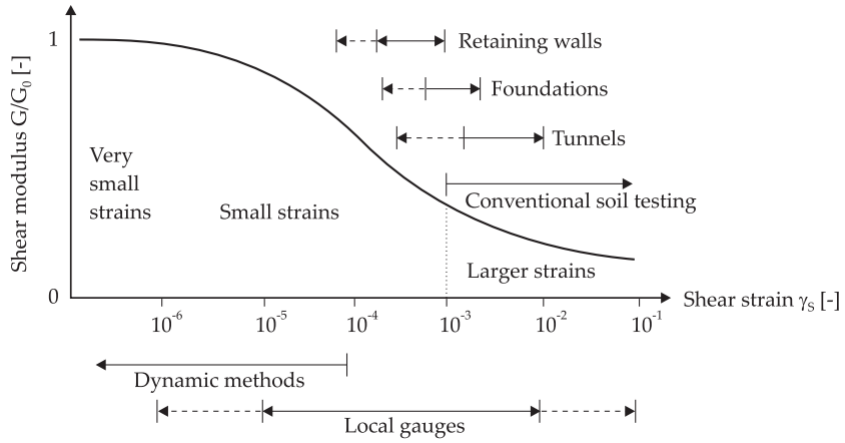

Figure 2.4: Characteristic stiffness-strain behaviour in logarithmic scale according to Atkinson and Sallfors (1991).

2.2.1 Parameters affecting v_s and G_0

"v_s in sands is controlled by the number and area of grain-to-grain contacts, which in turn depend on relative density, effective stress state, rearrangement of particles with age, and cementation" (Robertson, 2009).

In this section different physical sources of influence on v_s and G_0. As shown in chapter 2.1.1 the shear wave velocity depend upon a shear modulus G_0. In chapter 2.2 it was showed that the dynamic shear modulus and the small-strain shear modulus, G_{max}, is approximately equal ($G_0 \approx G_{max}$), and we can then see that the shear wave velocity and small-strain stiffness will be dependent variables, and expected to be affected by the same parameters.

There are many parameters affecting v_s and G_0. Benz (2007) ranked these parameters based on their relevance. This ranking is shown in figure 2.5. The parameters that are deemed very important for clean sands will be discussed further. The effect of some parameters are illustrated in figure 2.6.

Stain amplitude

As discussed earlier the strain stiffness decreases with increasing strain. Upon unloading, however, the soil immediately regains its initial stiffness (Benz et al., 2009). The decrease in stiffness can be approximated, which is the foundation for the plot given in figure 2.4, which shows the non-linear relation between stiffness and strain on a logarithmic curve.

Parameter	Importance to [a]			
	G_0		$\gamma_{0.7}$	
	Clean sands	Cohesive soils	Clean sands	Cohesive soils
Strain amplitude	V	V	V	V
Confining stress	V	V	V	V
Void ratio	V	V	R*	V
Plasticity index (PI)*	-	V	-	V
Overconsolidation ratio	R	L	R	L
Diagenesis*	V*	V*	R*	R*
Strain history*	R	R	V	V
Strain rate	R	R	R	R*
Effective material strength	L	L	L	L
Grain Characteristics (size,shape,gradation)	L*	L*	R	R
Degree of saturation	R	V	L	L*
Dilatancy	R	R	R	R

[a] V means Very Important, L means Less Important, and R means Relatively Unimportant

* Modified from the original table presented in Hardin & Drnevich[53]

Figure 2.5: Parameters affecting G_0 (Benz, 2007).

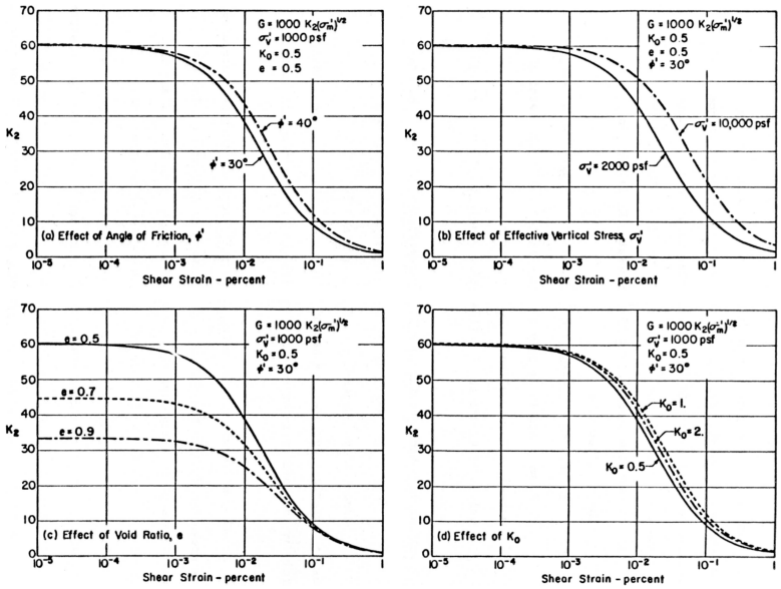

Figure 2.6: Effect of a) effective friction angle, (b) vertical effective stress, (c) void ratio and (d) K_0. Graphs are taken from Idriss and Seed (1970).

Confining stress

Hardin and Richart Jr (1963) proposed a relationship between small-strain stiffness and the confining pressure:

$$G_0 \propto (p')^m \tag{2.12}$$

where p' is the effective mean principal stress. Experience has shown that for non-cohesieve soils the exponent is in the range $0.40 \leq m \leq 0.55$ (Benz, 2007). It should also be noted that the confining stress influences the void ratio, and that a relation containing confining pressure also should account for the void ratio.

Void ratio

As seen from figure 2.6 the void ratio can have a drastic effect on the small-strain stiffness. Intuitively this makes sense if you think of wave propagation through a material. If the void ratio is small the grain-to-grain contact must be large, and the material will behave stiffer than if the void ratio were large. The most widely applied relation between void ratio and small-strain stiffness is proposed by Hardin and Richart Jr (1963), and given as:

$$G_0 \propto \frac{(2.17 - e)^2}{1 + e} \tag{2.13}$$

Other proposed relations are typichally given on the form (Benz, 2007):

$$G_0 \propto e^{-x} \tag{2.14}$$

Diagenesis

Diagenesis is used as a collective term and *" refers to the sum total of processes that bring about changes in a sediment or sedimentary rock subsequent to deposition in water"* (Berner, 1980). As a result of diagenesis we see that the stiffness of soils will become time dependent, i.e. $G = G(t)$. Most notable effects for our purposes is aging effects and cementation (Benz, 2007). Aging effect as a term can be indistinct, but mainly relates to changes in mechanical properties due to secondary compression under constant loading conditions, i.e. compression that takes place after the primary consolidation of a material. Cementation is a processes that involvs bridging between grains below the groundwater. Tests has shown that cementation in particular is important to the stiffness of sandy soils.

Chapter 3

Field methods

In this chapter relevant methods for measuring shear wave velocity in field will be presented. The methods chosen are those most relevant to the Øysand test site, both in terms of availability and usability. For this paper laboratory methods will not be discussed. One of the reasons for this is the uncertainty related to measuring shear wave velocity on sand in the laboratory. Benz (2007) observed that common sampling methods disturbed the sample to such a degree that when used for measurements in the laboratory the $G_{0,Lab}$ was as low as $0.25G_{0,Field}$.

3.1 Surface waves analysis

3.1.1 Multichannel analysis of surface waves (MASW)

MASW is a geophysical method of mapping the stiffness properties of soil in an 2D profile. The method is based on measuring the lower frequency surface waves in the range 3-30 Hz (Park et al., 2007). Execution of the test is easy and quick which makes it very economical compared to other field methods. It is also an non-intrusive test which means it does not damage the soil or need any excavation or boring to be performed. The method is however restricted to shallow depths, <30m, which primarily isn't a problem for geotechnical purposes.

The MASW method measures seismic activity through the use of multi-channel receivers which records the amplitude of surface waves (Park et al., 2007). The test is performed by placing the receivers (normally 24 or more) evenly spaced in a horizontal line on the surface, as shown in figure 3.1, connected to a seismograph.

For the active test a surface wave is actively generated, which creates a wave which propagates both along the surface and in the soil body. This is repeated at different predetermined positions along the horizontal line.

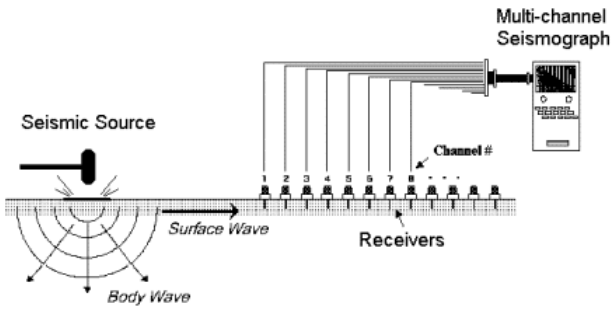

Figure 3.1: MASW method (Survey, 1998)

For each predetermined point multiple waves are generated, to ensure sufficient quality and quantity of measurements. For the passive test no wave is actively generated, but the "background noise" due to nearby sources is recorded over a longer time period. The recorded data from the passive and active test is then fed into software which analyzes the data, and returns a 2D-profile of the shear wave velocity.

3.2 Intrusive testing

Intrusive testing can be used as a common term for field methods where the seismic equipment is penetrated into the soil and waves are actively generated. The standard procedures for two of the methods presented in this section (SCPT and SDMT) both use similar sensors and methodology.

3.2.1 Seismic Dilatometer (SDMT)

The seismic dilatometer is a combination of the standard dilatometer and a seismic module for measurements of v_s. The standard dilatometer is a piece of equipment designed to measure the in-situ earth pressure at different depths. The earth pressure can further be related to other parameters, such as the material index (I_D), the horizontal stress index (K_D) and the dilatometer modulus (E_D) (Marchetti, 1980). For a thorough description of the DMT the reader is referred to literature by Marchetti (1980).

The seismic module on the SDMT consists of two sensors, placed 0.5m apart, which measures the shear wave. The test is instigated by the generation of a shear wave from the surface, as shown in figure 3.2. The shear wave is then recorded by the sensors. The mean shear wave velocity is then be found by taking the distance between the sensors and the difference in arrival time of the shear wave to the sensors, i.e the time it took for the wave to travel

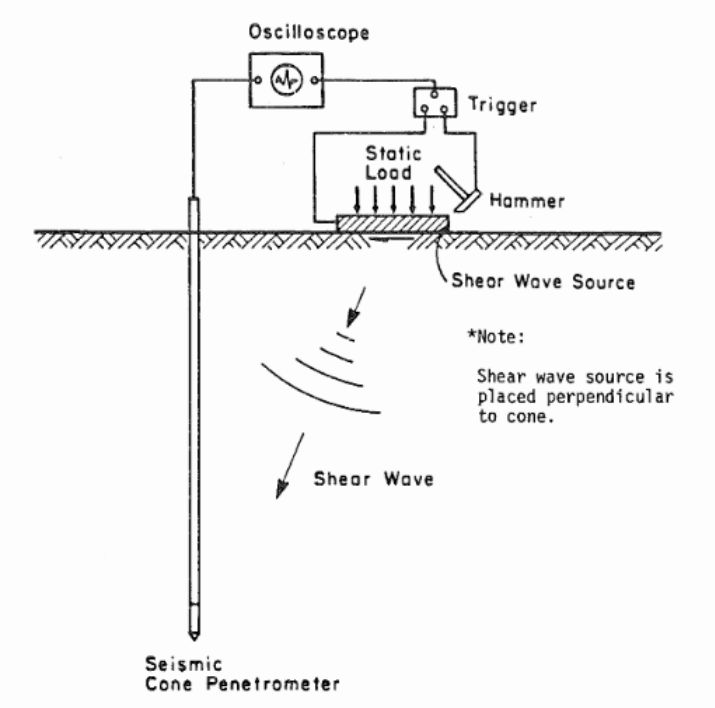

Figure 3.2: Methodology of SDMT and SCPT. Figure made by Robertson and Campanella (1983)

between sensor 1 and sensor 2 (Marchetti et al., 2008). For each depth multiple measurements are made, and the average reading is used to estimate v_s. Measurements are usually taken at regular depth intervals.

3.2.2 Seismic Cone Penetration Test (SCPT)

The SCPT uses the same principles for measuring the shear wave velocities as the SDMT (Robertson et al., 1986). The main difference is only that the seismic module is placed on a CPT instead of a DMT. One advantage of the SCPT compared to the SDMT is that CPT is a more common test, and the seismic test doesn't require separate tests that would not have been carried out initially.

3.2.3 Crosshole Testing (CHT)

Crosshole testing is a method for in-situ measurements of p- and s-waves. The procedure of CHT is based on the generation of waves for sending of energy waves between two or more boreholes. This is done by drilling two vertical boreholes in close proximity. A source within the rod in the first borehole creates a signal that is sent into the surrounding soil, creating shear waves and p-waves (see figure 3.3). The signal is then recorded as it arrives at the rod in the other boreholes. This is done for multiple depths (Benz, 2007).

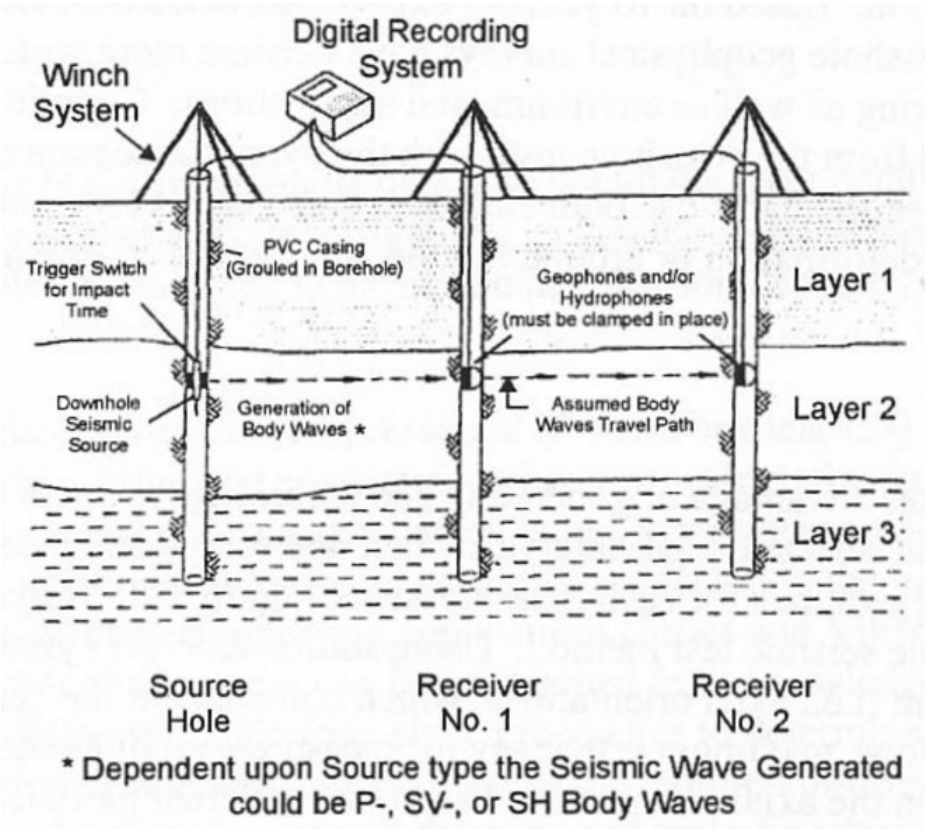

Figure 3.3: Methodology of Crosshole testing. Figure by EPA (2016)

From the recorded signal the shear wave velocity can be calculated. It is important that the source signal and the receiver is at the same depth. It should also be noted that this method is most useful for measurement in soils with horizontal layering (EPA, 2016).

For most purposes crosshole tomography has today replaced the traditional crosshole test. In the tomography test the single receiver-sensor is replaced by a string of sensors, receiving at relative depths to the source (Benz, 2007). This way multiple ray paths can be calculated, and uneven layers can also be measured. A result of this method is the ability to use inversion techniques to produce a 2D profile of shear-wave velocity or stiffness of the soil. An example of a 2D soil profile is given in figure 3.4.

CHT is one of the most reliable methods for in-situ measurement of the shear wave velocity and small-strain stiffness (Benz, 2007). It should also be noted that CHT is one of the most expensive tests for measuring the shear wave velocity. Due to the interpretations dependency of the distance between the boreholes it is of vital importance that the distance is determined exactly. One way to insure this is by using inclinometers inside each borehole to measure how much each rod strays out of bound.

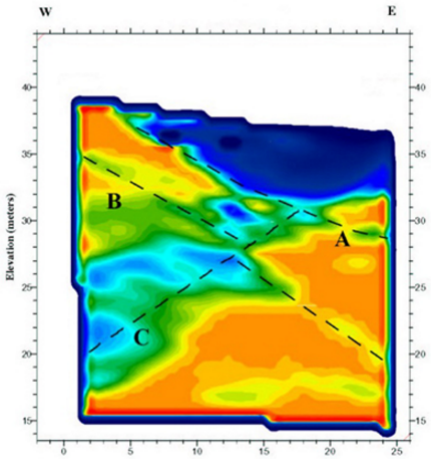

Figure 3.4: Example of 2D soil profile. Figure by GeoScience (1999)

Chapter 4

Pilot project at the Øysand site

This chapter aims to give a quick introduction to the Øysand test site with respect to location and soil classification.

4.1 Location

The chosen sand-site for the NGTS is Øysand in the municipality of Melhus in Sør-Trøndelag. The site is located approximately 5km south of Trondheim and is shown on the map in figure 4.1. The topography of the area is relatively flat, and the site is in close proximity to both the Trondheim fjord and the estuary of the river Gaula.

Figure 4.1: Overwiev map of the test site.

Borehole	*Depth*	*ID*	*Soil type*
7	7-8m	A	Clayey sand
9	2m	B	Sand Medium graded
9	4-5m	C	Sandy, gravelly, clayey Well graded
9	5-6m	D	Sandy, gravelly, clayey Well graded
9	6-6,6m	E	Sandy, gravelly, clayey Well graded

Table 4.1: Selected results from laboratory tests.

4.2 Classification

Classification of the soils at Øysand is important. We need to know what kind of material we have, to determine what kind of behaviour to expect from the soil. This section will therefore be devoted to a discussion of the classification of the soils at Øysand.

4.2.1 Geological Survey of Norway

The mapping service by the geological survey of Norway has been used to provide a rough overview of the general sorts of sediments for the area (NGU, 2016). For the entire area one can expect dominance of river deposits, with some thick ocean deposits. For river deposits one would expect a large presence of sand and gravel (Mjaavatten, 2007).

4.2.2 Laboratory test

The author of this paper has also performed some laboratory test to determine the grain size distribution for different soil samples. Tests have been performed on five samples, four from borehole 9 and one from borehole 7. The tests performed is sieving, hydrometer and visual inspection. Results are given in appendix C. Selected results from the laboratory tests are given in table 4.1. The table shows that the general classification for all samples is of a high sand content, with some silt and/or clay.

4.2.3 CPTU classification

Soil classification can also be performed by interpretation of results from CPT. Robertson (1990) suggested two charts for soil classification, which incorporates three-dimensional CPTU data. The charts uses normalized cone

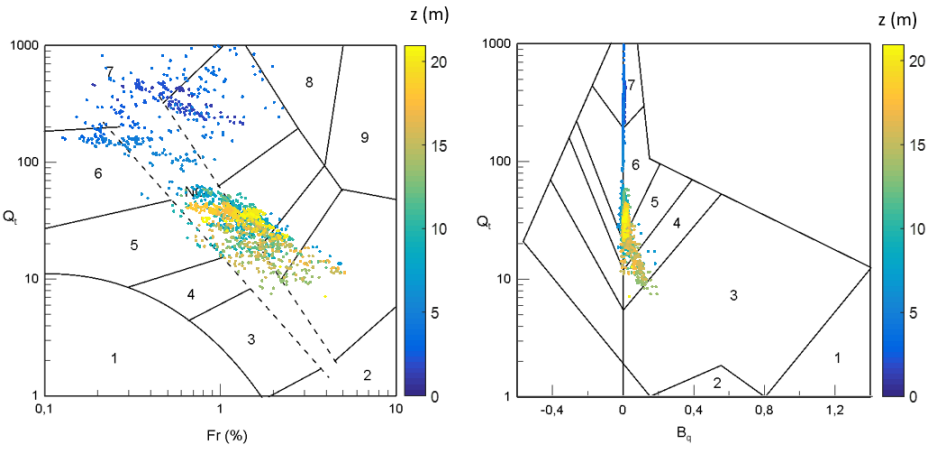

(a) Soil classification charts CPTU Borehole 9. Chart provided by NGI.

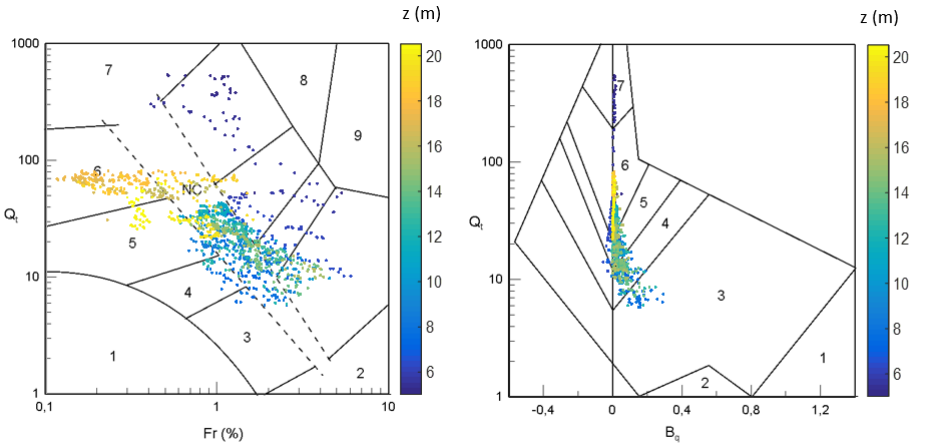

(b) Soil classification charts CPTU Borehole 16. Chart provided by NGI.

resistance (Q_t), normalized friction ratio (F_r) and the pore pressure ratio (B_q). By normalizing all factors the influence of for example overburden stress is taken into account. Tom Lunne (1997) emphasize the fact that these charts are global in nature, which means they only provide a guide to soil classification and should be combined with local experience and tests.

By examining the charts from the CPTU-tests performed, figure 4.2a and 4.2b, we can make a rough estimate of the soil classification. It is evident that for borehole 9 there is a lot of sand. The chart classifies most of the profile as clean sand or silty sand, which fits well with the results from the lab. The deeper we get, the more silt it seems to be in the sample. At the top of the profile the chart indicates that there should be more gravel, which seems fair.

The classification of borehole 16 gives mainly classification as different sand mixtures, but with a higher silt and clay content, and is in parts classified completely as clayey silt or silty clay. This indicates that there might be more layering in borehole 16. Since we have made no laboratory tests on samples from near borehole 16 it is hard to evaluate the accuracy of this classification.

Zone	Soil Classification
1	Sensitive fine grained
2	Organic material - clay
3	Clay
4	Silty clay to clay
5	Clayey silt to silty clay
6	Sandy silt to clayey silt
7	Silty sand to sandy silt
8	Sand to silty sand
9	Sand
10	Gravelly sand to sand
11	Very stiff fine grained
12	Sand to clayey sand

Table 4.2: Interpretation of soil classification charts (Robertson, 1990)

4.2.4 Conclusion

From evaluating the soil by both laboratory methods and through CPT-classification it seems to be fairly clear the site is dominated by sand, with parts consisting of finer materials. As seen in appendix C all test samples has a sand content larger than 40%, and at the most it more than 90% sand. It is still somewhat unclear how the distribution is around borehole 16, and whether we can assume somewhat the same distribution.

Chapter 5

Correlations

As shown in the chapter 3 there exists many ways of determining the shear wave velocity and the small-strain stiffness in-situ quite accurately for soils. There is however an extensive effort being made to correlate these parameter to the results from more common tests, such as the standard CPT. By estimating these parameters by empirically based correlations one could produce more results, and avoid time consuming tests spent on each specific parameter.

The correlations presented in this section are all made under given conditions and assumptions. Common for all are that they are estimated on sand. Many correlations can be said to be site-specific and must therefore always be corrected for the sites you want to use them on. However a lot of work has been put into collecting such site-specific correlations, and establishing more or less general relations. In this chapter two different CPT-correlations will be presented.

5.1 Foundation for CPT-correlations

Many correlations for determining shear wave velocity by CPT-measurements has been made through the years. Many of these are site-specific and therefore non-general. In an article by Rix and Stokoe (1991) they state that: *"(...) G_{max} and q_c depend on the state stress and density to different degrees, making a unique correlation between them impossible"*. They also suggest that there might be factors affecting the parameters that these correlations do not include, and hence the correctness of correlations will differ. There has, however, been made efforts to determine more general correlations by Andrus et al. (2007), Robertson (2009) and others. These methods commonly use normalized and dimensionless cone parameters, proposed by Robertson (1990):

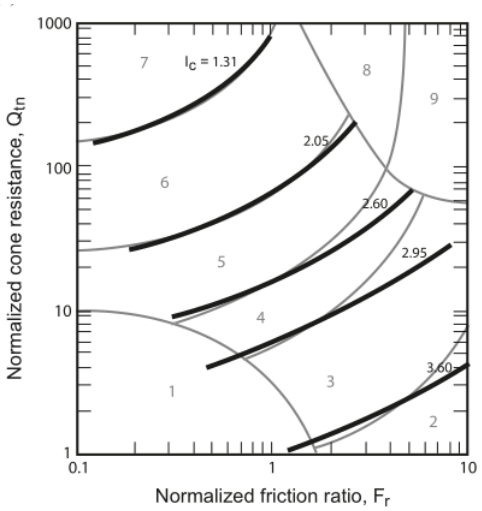

Figure 5.1: Contours of soil behaviour index on normalized SBT $Q_{tl} - F_r$-chart. Figure made by Robertson (2009).

$$Q_{tl} = (q_t - \sigma_{v0})/\sigma'_{v0} \tag{5.1}$$

$$F_r = [f_s/(q_t - \sigma_{v0})]100 \tag{5.2}$$

$$B_q = (u_2 - u_0)/(q_t - \sigma_{v0}) \tag{5.3}$$

Commonly used is also the Soil behaviour type index, I_c. This value is used to approximate the boundaries in the normalized SBT $Q_{tl} - F_r$-chart (see chapter 4.2.3), and is used to modify empirical correlations that varies with soil type. The index is given as:

$$I_c = [(3.47 - logQ_{tl})^2 + (logF_r + 1.22)^2]^{0.5} \tag{5.4}$$

5.1.1 Correlation 1: Proposed by Robertson (2009)

Assuming coarse-grained soils and drained conditions Robertson (2009) proposed correlations between normalized CPTU-measurements, shear wave velocity and small-strain stiffness. The proposed correlations are based on over 100 SCPT-profiles from 22 sites in California, and have further been evaluated and verified using publish material from other sites around the world (Robertson, 2009). The correlation is based on the development of a normalized shear velocity, v_{sl}, using the normalized SBT $Q_{tl} - F_r$-chart (see chapter 4.2.3), from the measurement of shear wave velocity by a SCPT. The relationship between the normalized shear wave velocity and the measured value, is defined as:

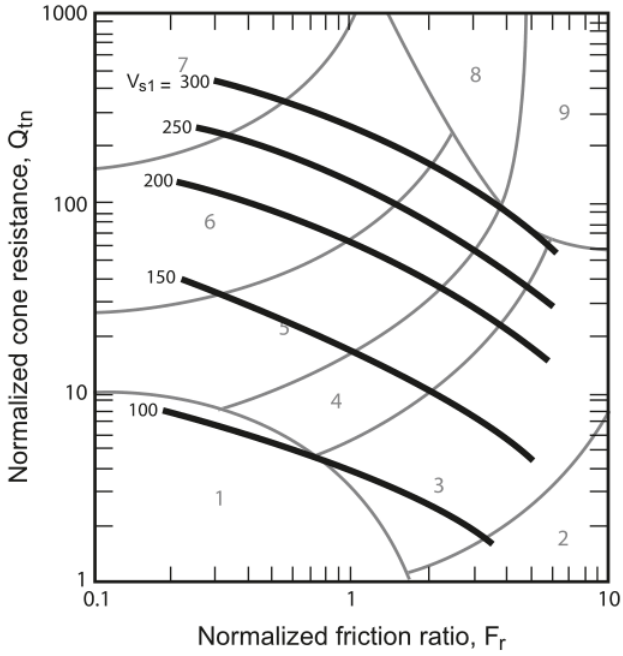

Figure 5.2: Contours of normalized shear wave velocity on normalized SBT $Q_{tl} - F_r$-chart. Chart made by (Robertson, 2009)

$$v_{sl} = v_s(\frac{p_a}{\sigma'_{v0}})^{0.25} \tag{5.5}$$

At this point we introduce a shear wave velocity cone factor. This factor approximates the relationship between the normalized SBT $Q_{tl} - F_r$-chart and v_{sl}, shown in figure 5.2. This yields the following relationship equation for shear wave velocity:

$$v_s = [\alpha_{vs}(q_t - \sigma_v / p_a]^{0.5} \tag{5.6}$$

where:

$$\alpha_{vs} = 10^{0.55 I_c + 1.68} \tag{5.7}$$

This approximation of the shear wave velocity has proved to be pretty good. However, Andrus et al. (2007) showed that the error of the approximation increased with the age of the deposit, and that the method generally underestimates the shear wave velocity of Pleistocene-age deposits.

5.1.2 Correlation 2: Proposed by Andrus et al. (2007)

Working under the assumption of a empirical relationship between the shear wave velocity and the normalized CPT-values, Andrus et al. (2007) created

a set of empirical correlations which incorporates aging effects. The correlations are based on evaluation of 229 pairs of data from across the world, where the age of the soils range from Holocene (<10,000 years), Pleistocene (10,000-1.8 million years) to Tertiary (1.8-60 million years). Some of the requirements that where made for the sites in the database was that measurements had to be taken below groundwater, at sites where reasonable approximations of effective vertical stress could be made, and that measurements were from thick uniform layer. All models were created through regression analyses.

For Holocene-age soils the most relevant empirical model is given as:

$$v_s = 2.27 q_t^{0.412} I_c^{0.989} z^{0.033} ASF \tag{5.8}$$

where ASF is an age scaling factor, which is set as 1.0 for Holocene-soils. Coefficient of determination is found to be $R^2 = 0.779$.

For Pleistocene-age soils the most relevant empirical model is given as:

$$v_s = 2.62 q_t^{0.395} I_c^{0.912} z^{0.124} SF \tag{5.9}$$

where SF is an scaling factor, which is set as 1.11 for Pleistocene-soils. Coefficient of determination is found to be $R^2 = 0.430$.

Chapter 6

Results

In this chapter the results from the field tests will be presented shortly, and the correlations presented in chapter 5 will be tested, and their results will be discussed.

6.1 Field tests

For this pilot project CPTU, SDMT and MASW field test has been performed. SDMT and MASW has been done to measure directly the values of the shear wave velocity, while the CPTU was done without the seismic part, and must therefore be correlated to find shear wave velocities.

6.1.1 SDMT

One SDMT has been performed at the Øysand site at borehole 9 (see map in appendix F). The SDMT was taken in two parts, first between 1.10m and 2.55m, and then between 6.5 and 17.0 meters. Between 2.55m and 6.5m the drill encountered a coarse hard layer which proved difficult to penetrate with the SDMT equipment. This part then had to be predrilled. The measurements were taken for every 50cm, and at every borehole multiple readings were made. Result from the test is shown in figure 6.1, alongside the results from the MASW.

6.1.2 MASW

Two MASW test has been performed at two different locations on the test site. The location of the tests are given in the map in appendix G. The resulting interpretated shear wave velocity is given in figure 6.1. From the figure it seems that no clear connection between the values from the SDMT and the MASW.

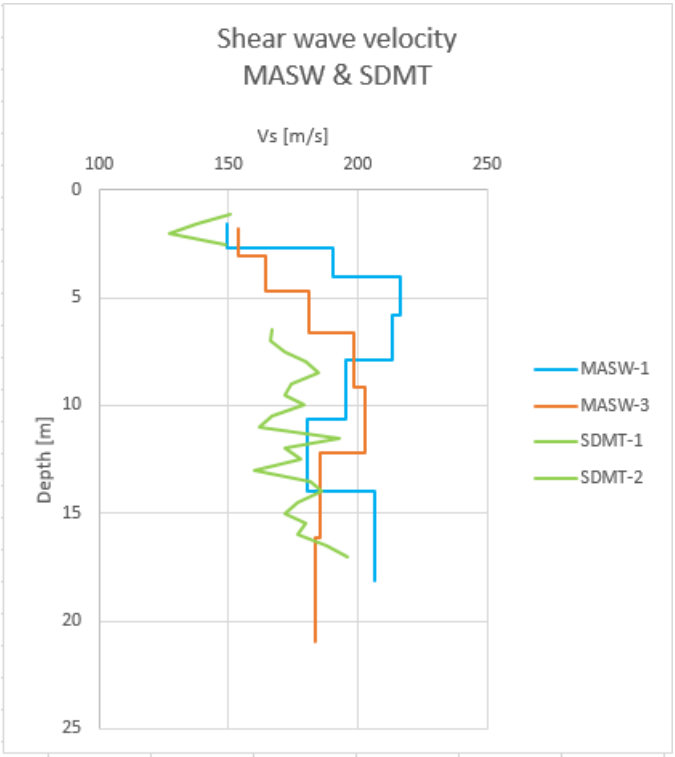

Figure 6.1: Comparison of results from MASW and SDMT

6.1.3 CPTU

Two CPTUs has been performed at two different locations on the test site. The tests were performed at borehole 9 and 16 (see map in appendix F). The CPTUs were performed without an seismic part. Results from the CPTUs are given in appendix H.

6.2 CPT-correlations

6.2.1 Results

Estimations of the shear wave velocity has been made on the models of Robertson (2009) and Andrus et al. (2007), presented in chapter 5. The estimations are made on CPT-results from both borehole 9 and 16. The estimations are then compared with the assumed correct value, i.e. the measured shear wave velocity from the SDMT. Two plots are given. The first plot is of shear wave velocity over depth (see figure 6.2). The other plot is a comparative plot which evaluates the performance of the $CPT - v_s$ correlation and is given in figure 6.3 to 6.6.

Studying the plots in figure 6.2 for borehole 9 one can see that the predicted values fit pretty good with the measured values. The first 8m the pre-

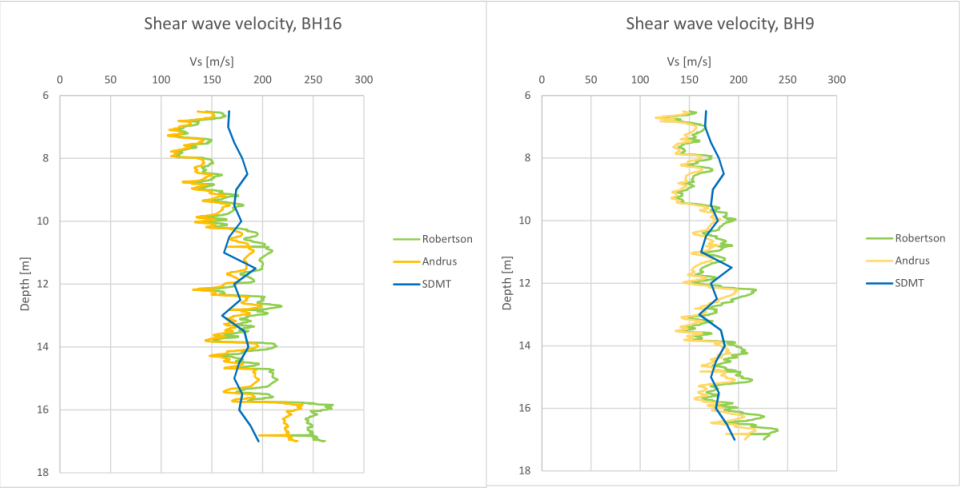

Figure 6.2: Comparative plot of the SDMT-values and the chosen correlation-models on CPT

diction seems to underestimate the shear wave velocity, but after that the trendline of the predictions seems to fit well with the measured values, with more scatter of course. It is also notable that both predictions follow the same path, only with different amplitudes in the scatter, which is reasonable seeing as they both depend on the CPT-values. Looking at the comparative plots, figure 6.3 and 6.5, from borehole 9 we also see that both correlations seem to do adequately well in predicting shear wave velocity. Observe that the correlation proposed by Andrus et al. (2007) have more points with an error above 20% than the correlation proposed by Robertson (2009), but it also has more points of approximately exact fit, i.e. on the middle line.

For borehole 16 we see more error compared with the measured SDMT data. This doesn't necessarily mean that the predictions are bad, but that the measured SDMT values may not extrapolate so easily to the location of borehole 16. This statement is supported by investigating figure 6.4 and 6.6. In chapter 4 it was indicated the the soil classification may not be completely similar in borehole 9 and 16, and we should therefore expect different results from the estimations. We should then disregard the CPT-estimations from borehole 16, since they give no sure indication on whether the proposed CPT-correlations can be used.

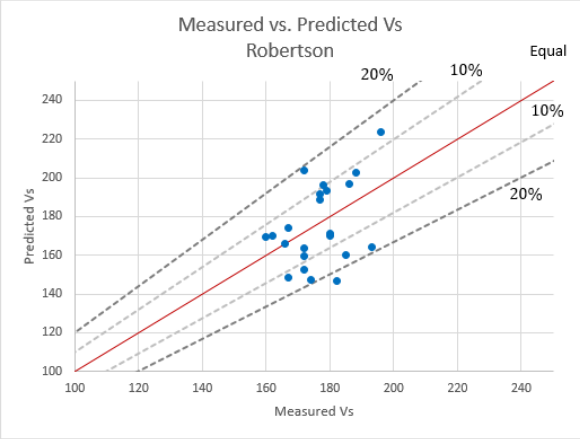

Figure 6.3: Robertson, BH 9

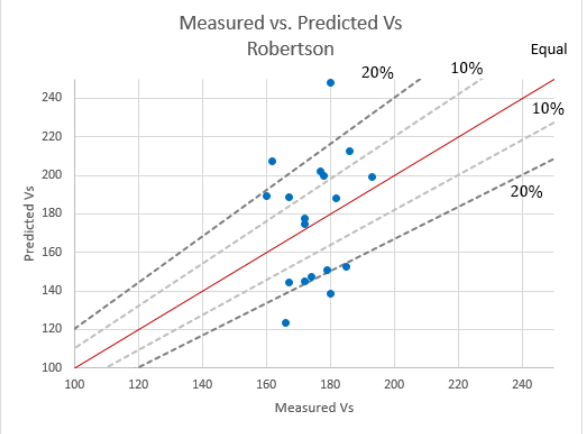

Figure 6.4: Robertson, BH 16

Figure 6.5: Andrus, BH 9

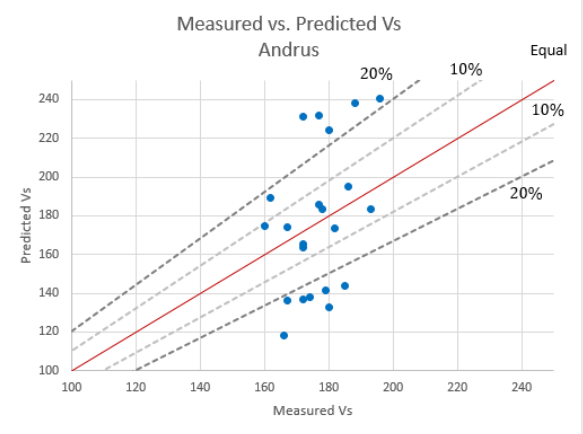

Figure 6.6: Andrus, BH 16

Chapter 7

Summary and Recommendations for Further Work

In this study the theoretical foundations within geodynamics and wave propagation has been investigated. Shear waves are defined as distortional waves, i.e. waves that only produces shearing and no voluminal change. Shear wave velocity depends mainly on the strain amplitude, confining pressure, void ratio and diagenesis, wheras void ratio is one of the most influential. These parameters should all be represented in one way or another in empirical relations trying to relate to shear wave velocity.

The pilot study at the Øysand site concludes that the soil is mainly sand with varying contents of clay and silt. The laboratory test gave consistent results, and were backed up by soil classifications from CPTU and data from the Geological Survey of Norway.

The proposed correlations used to estimate the shear wave velocity seem to perform quite adequately for the Øysand test-site. However, the amount of data for the comparisons is quite small and it is hard to make a statistical significant evaluation of the correlations on the basis of the gathered data. Only one SDMT has been performed and the results from the MASW is relatively crude and works mainly as an estimation of shear wave velocity rather than a basis for evaluation of correlations. The concluding statement may be that both correlations seem to produce good results, but further investigations should be performed to increase the sample size.

For further work the author recommends that there should be perform more seismic investigations on the Øysand site. These investigations should be complimented with the calculations of more values from correlations, and ultimately result in the establishment of a site-specific correlation for the Øysand site based on regression analysis. Efforts could also be made to determine values for void ratio and confining pressure at the sites, so correlations that isn't CPT-based may be tested.

Appendix A

Acronyms

CHT Crosshole testing

CPT Cone Penetration Test

NGTS National Geo-Test Sites

MASW Multichannel analysis of surface waves

SCPT Seismic Cone Penetration Test

SDMT Seismic Dilatometer

Appendix B

List of symbols

B.1 Letters

ASF Age scaling factor

B_q Pore pressure ratio

e Void ratio

E Youngs modulus

F_r Normalized friction ratio

f_s Unit sleeve side friction ratio

G Shear modulus

G_0 Small-strain stiffness

$G_{0,Lab}$ Small-strain stiffness measured from lab

$G_{0,Field}$ Small-strain stiffness measured from field

G_{max} Small-strain stiffness

I_c Soil behaviour index type

p' Mean stress

p_a Reference stress = 100 kPa

q_t Corrected cone resistance

Q_{tl} Normalized cone resistance

SF Scaling factor

u_0 In-situ pore pressure

u_2 Pore pressure measured behind cone of CPTU

v_p P-wave velocity

v_s Shear-wave velocity

v_{sl} Normalized shear-wave velocity

z Depth

B.2 Greek symbols

α_{vs} Shear wave velocity cone factor

$\tilde{\epsilon}$ Volumetric strain

λ Lamé's constant

ν Poisson's ratio

ρ Material density

σ_{v0} Total overburden stress

σ'_{v0} Effective overburden stress

σ_{ij} Shear stress in direction ij

σ_{ii} Normal stress in direction ii

∇ Laplacian operator

Appendix C

Classification of Øysand soil

A classification of the Øysand soil has been made by the author of this paper. The test performed are sieving, hydrometer and visual classification. The tests were performed in accordance with ASTM standards and norwegian standards. Classification was made of five soil samples, four from borehole 9 and one from borehole 7. The boreholes are located approximately 75m apart, and their location is given in appendix F. The depth of the samples are given in tabel C.1 and C.2. The samples were given id A through E. In this chapter important results from this classification will be presented.

C.1 Visual classification

A visual description has been made of the soil. The description is made immedeatly after the sample is opened in the laboratory, i.e. it has not been altered or dried. The descrition was performed in accordance with the ASTM standard D2488-09a (ASTM, 2000). The description is given in table C.1.

C.2 Grain-size distribution

Both sieving and hydrometer test has been performed for all samples. The tests has been performed in accordance with ASTM standard D422-63 (ASTM, 2007). Important values from the grain-size distribution is presented in table C.2. The grain-size distribution curves are given in appendix D.

C.3 Discussion of error

From studying the grain-size distribution curves in appendix D it is clear that for sample C, D and E the curve drops radically when the curve goes into the

[1] In accordance with Vegvesen (2005)

Borehole	***Depth***	**ID**	***Visual description***
7	7-8m	A	Rounded, with some flat and elongated gravel particles. High sphericity. Brown and gray, with a sort of golden color. The sample was moist, with weak cementation. Seems to be a medium to coarse sand. Largest gravel particle was approx. 2x1x1.5cm3
9	2m	B	Subrounded, with some flat and elongated gravel particles. Low sphericity. Mainly gray and brown. The sample was wet with weak cementation. Seems to be a coarse sand. Largest gravel particle was approx. 2x1x0.5cm3
9	4-5m	C	Subangular, in general not flat or elongated, but examples of both. Mainly gray with a little brown. Coarse to medium sand. Largest gravel approximately 5x2x3cm3
9	5-6m	D	Subangular, in general not flar or elongated. Mainly gray, brownish. Seems like approx. 20% gravel. Coarse to medium sand, some clay. Maximum size of gravel: 2x2x2cm3
9	6-6,6m	E	Subangular. Mainly gray. Approx. 15% gravel, with coarse to medium sand, and some clay. Largest particle (Gravel) is 1x1x1cm3.

Table C.1: Visual classification of soil samples

			Sieve				**Classification**	
Borehole	***Depth***	***ID***	***% Fines***	***% Coarse***	***% Sand***	***% Gravel***	***Cu***	***Soil type***[1]
7	7-8m	A	6,59 %	93,41 %	90,53 %	2,88 %	4	Clayey sand
9	2m	B	3,78 %	96,22 %	81,62 %	14,60 %	6	Sand Medium graded
9	4-5m	C	7,58 %	92,42 %	47,69 %	44,73 %	40	Sandy, gravelly, clayey Well graded
9	5-6m	D	11,88 %	88,12 %	58,23 %	29,89 %	27,1	Sandy, gravelly, clayey Well graded
9	6-6,6m	E	13,33 %	86,67 %	63,71 %	22,96 %	23,1	Sandy, gravelly, clayey Well graded

Table C.2: Results from grain-size distribution tests

area for the hydrometer, i.e. grain size is below $75\mu m$. It is safe to assume that there must have been done some errors in the execution of the tests. In hindsight it is worth noting that the soils, once dispersed in a solution of sodium pyrophosphate, flocculate and bind into a soft mass. Before initiating the test the soils were mixed, both by a stirring apparatus and manually by shaking the sedimentation cylinder. It is vital that a visual inspection of the sedimentation cylinder is made before starting the test, to ensure that the material has not flocculated at the bottom. This was not done for sample C, D and E, and this might be the reason for the strange results. If the coarse section of the soil has flocculated at the bottom, the test will not detect the correct portion of this section.

The laboratory tests was performed in accordance with the ASTM standards. However it was later decided that the NGTS-project were to use the Norwegian standards (NS 8005). The methodology in these standards are very similar, but it may still lead to some differences. For example all material smaller than 2mm were not wet sieved as stated in NS8005 (1990), but dry sieved.

Appendix D

Grain-size distribution curves

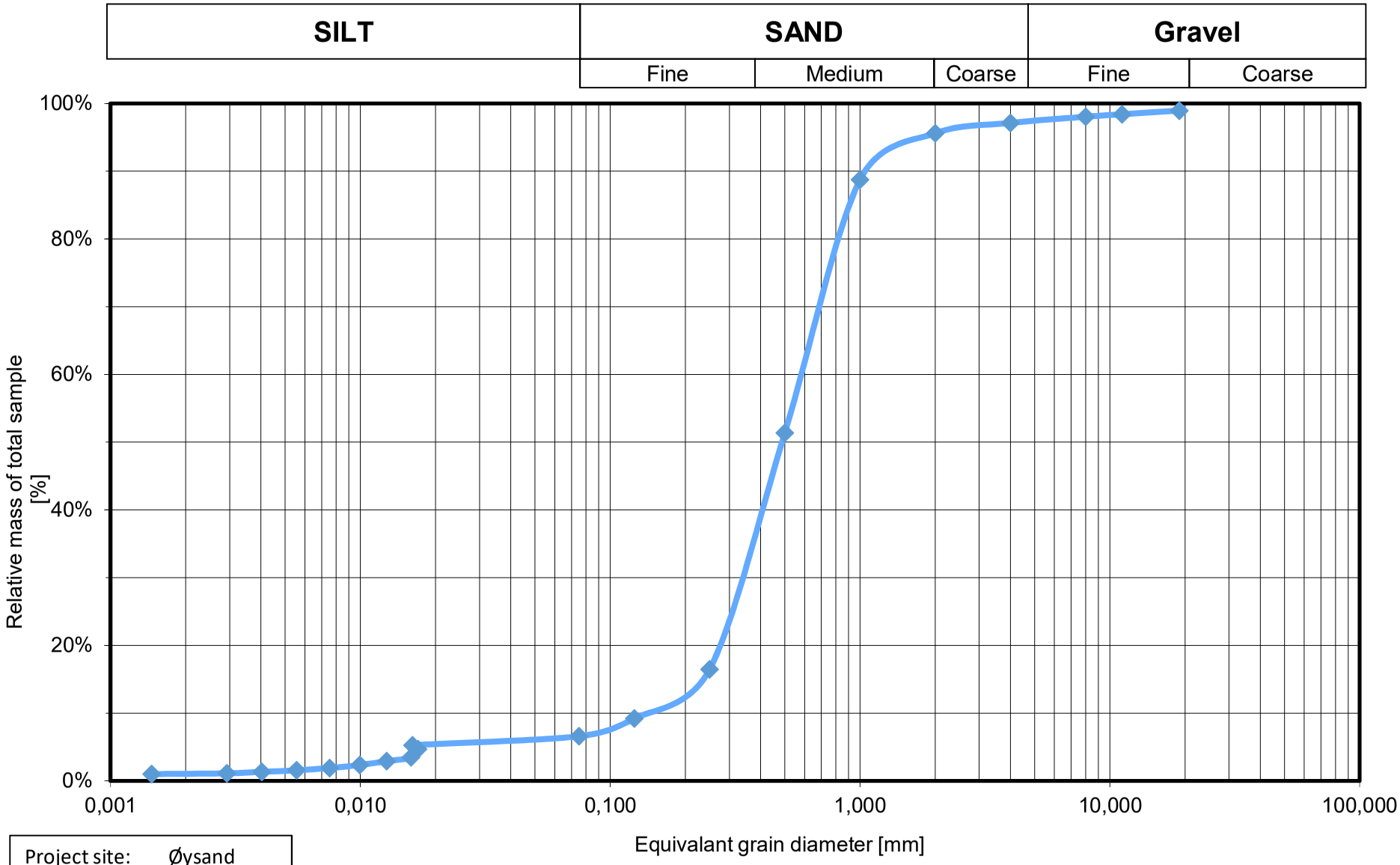

Project site: Øysand
Borehole nr.: 9 (7-8m)
Type of sample: Bag

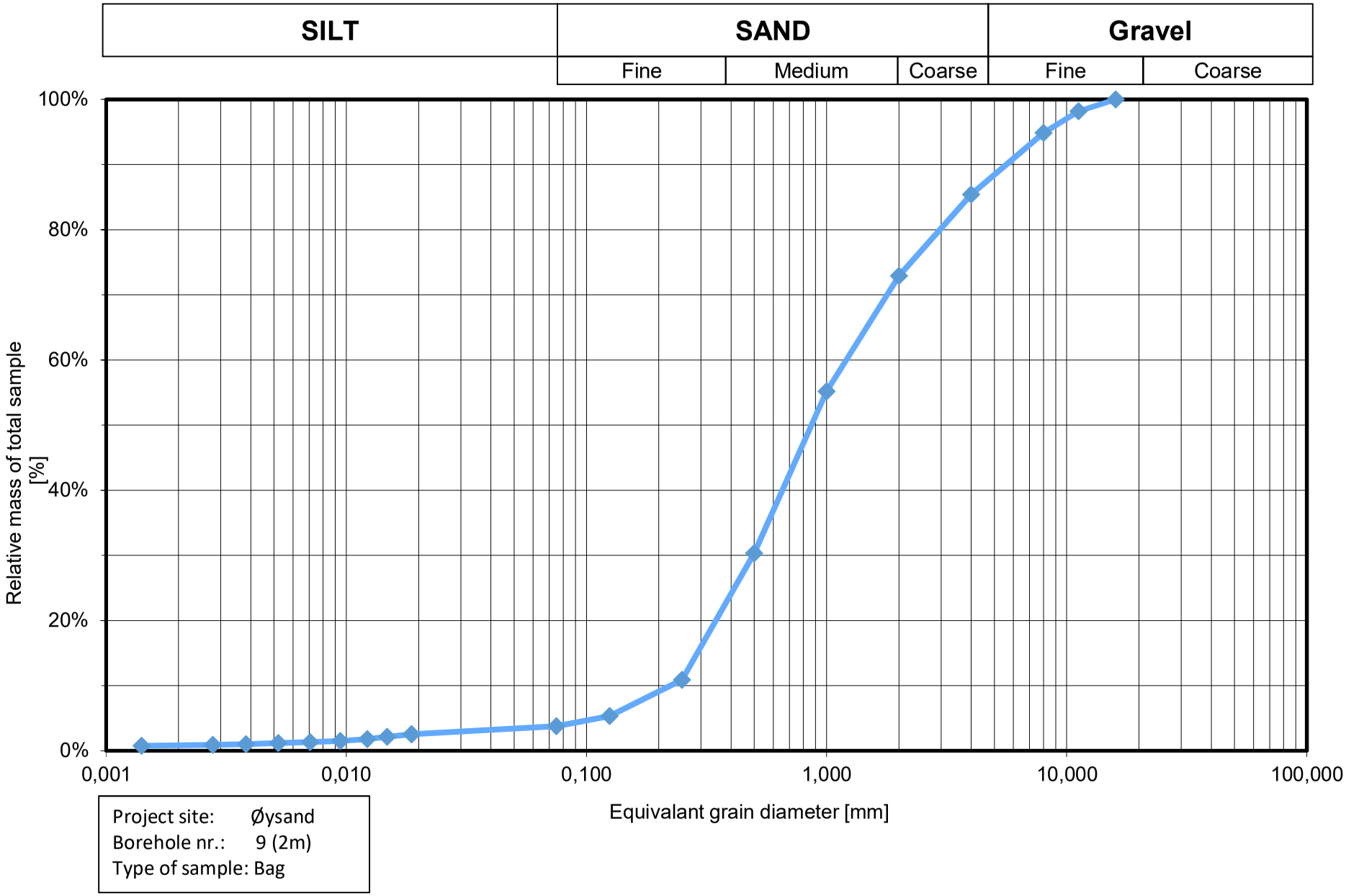
SILT
SAND
Gravel
Fine
Medium
Coarse
Fine
Coarse
100%
80%
60%
40%
20%
0%
Relative mass of total sample [%]
0,001
0,010
0,100
1,000
10,000
100,000
Equivalant grain diameter [mm]
Project site: Øysand
Borehole nr.: 9 (2m)
Type of sample: Bag

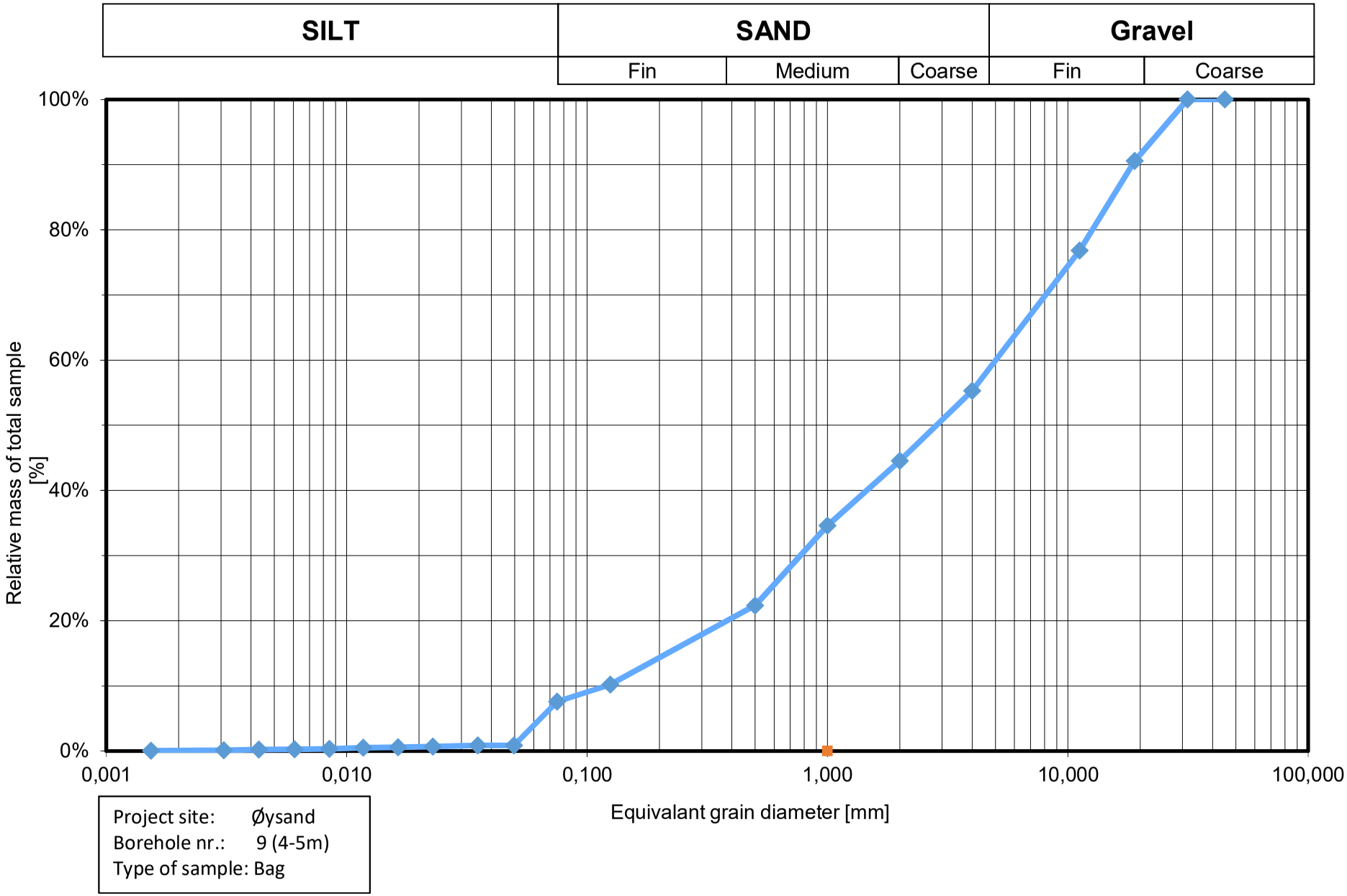
SILT
SAND
Gravel
Fin
Medium
Coarse
Fin
Coarse
100%
80%
60%
40%
20%
0%
Relative mass of total sample [%]
0,001
0,010
0,100
1,000
10,000
100,000
Equivalant grain diameter [mm]
Project site: Øysand
Borehole nr.: 9 (4-5m)
Type of sample: Bag

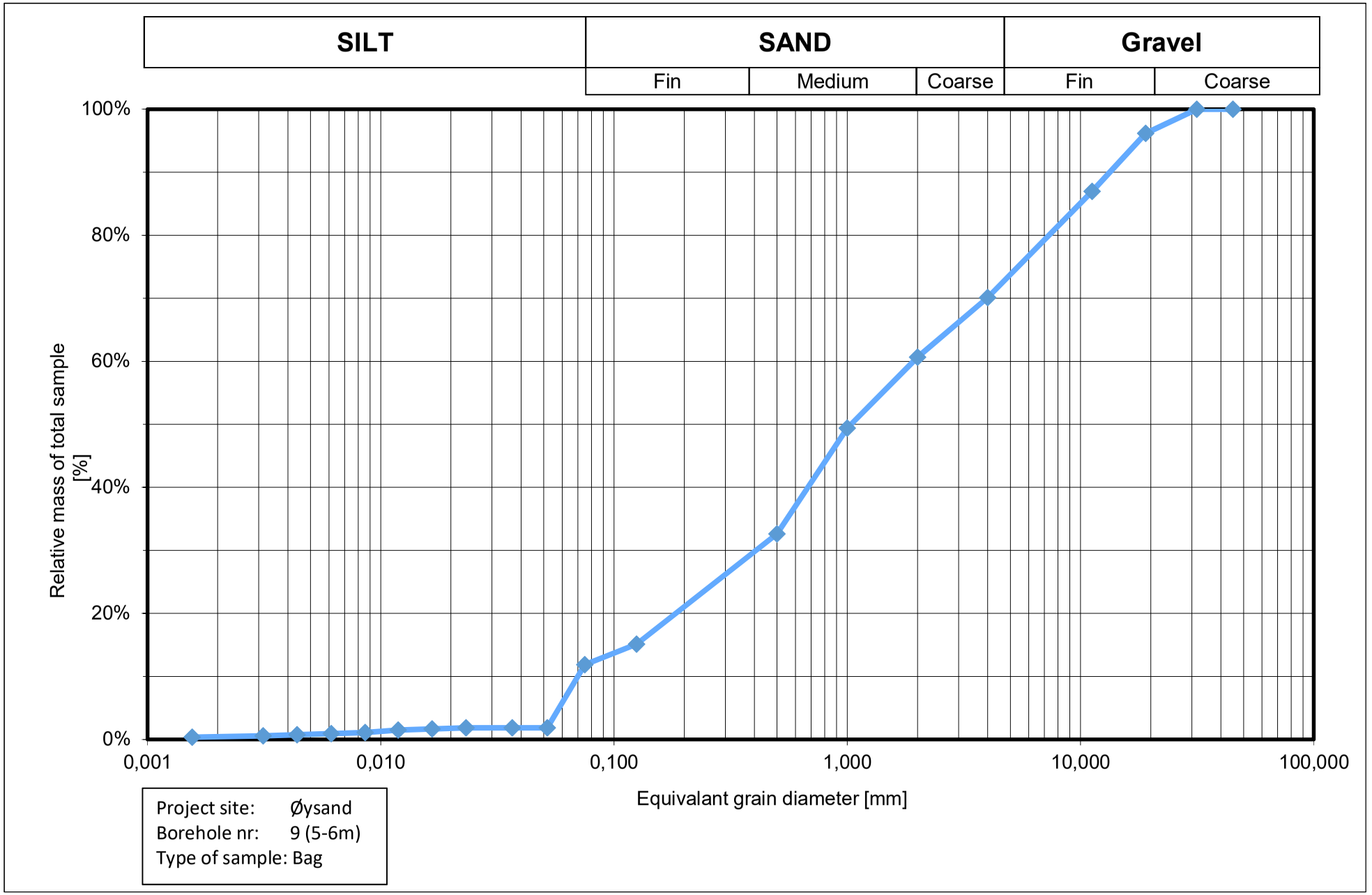
SILT
SAND
Gravel
Fin
Medium
Coarse
Fin
Coarse
100%
80%
60%
40%
20%
0%
Relative mass of total sample [%]
0,001
0,010
0,100
1,000
10,000
100,000
Equivalant grain diameter [mm]
Project site: Øysand
Borehole nr: 9 (5-6m)
Type of sample: Bag

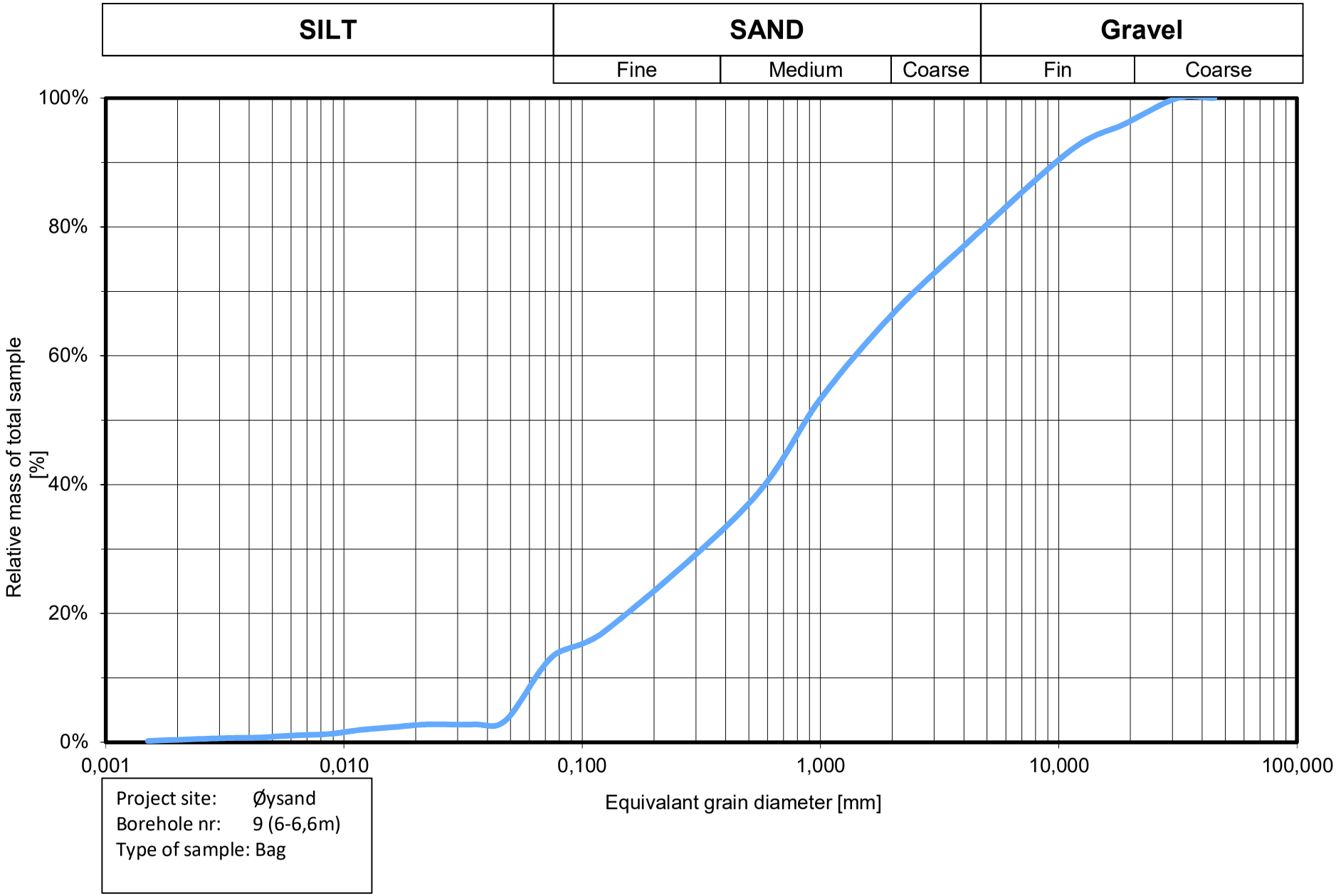
SILT
SAND
Gravel
Fine
Medium
Coarse
Fin
Coarse
100%
80%
60%
40%
20%
0%
Relative mass of total sample [%]
0,001
0,010
0,100
1,000
10,000
100,000
Equivalant grain diameter [mm]
Project site: Øysand
Borehole nr: 9 (6-6,6m)
Type of sample: Bag

Appendix E

SDMT Results Borehole 9

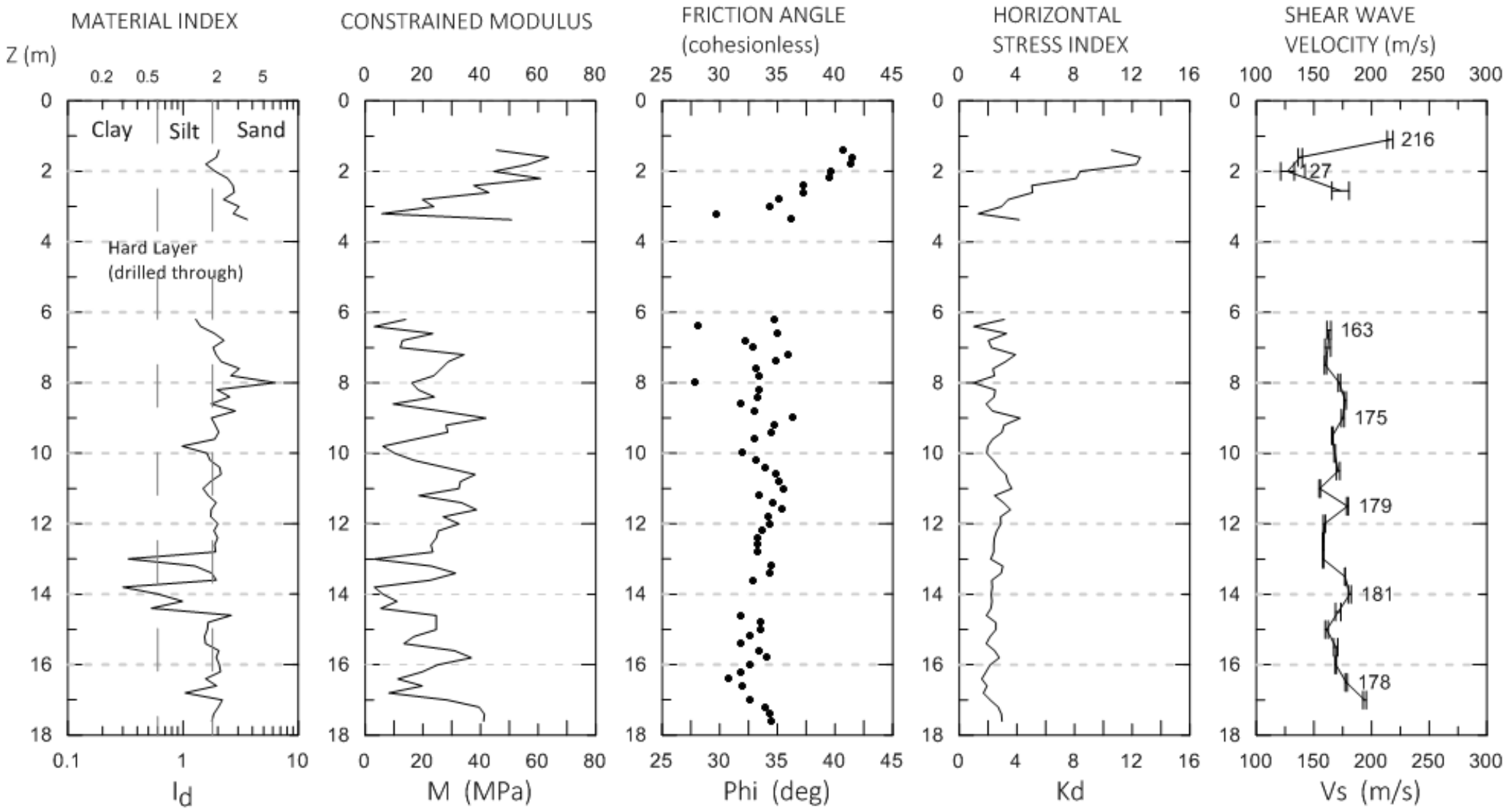

Legend

SDMT - 1

SDMT - 2

NGTS Sand Site - Øysand

Seismic Dilatometer Test at Sounding #9

SDMT - 1: conducted on Oct. 27, 2016

SDMT - 2: conducted on Nov. 2, 2016

Document No.
20160154-XX-X

Figure No.
001

Date
2016-11-10

Drawn by
ZeO

NGTS

P:\2016\01\20160154\Sand Site\Field investigations\Øysand\SDMT\Id_M_cu_phi_Kd plot.grf

Appendix F

Map of borehole placement

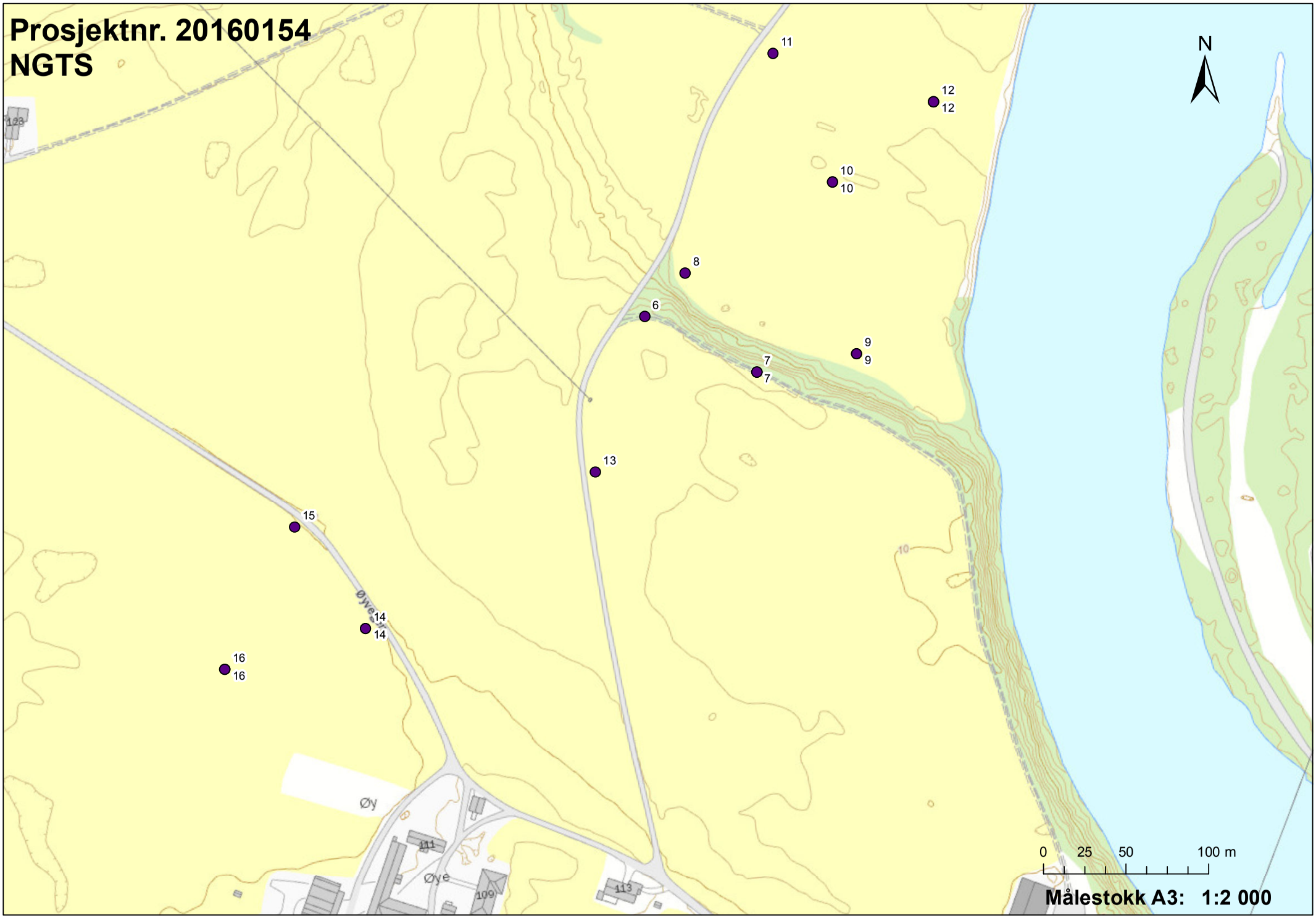
Prosjektnr. 20160154
NGTS
N
11
12
12
10
10
8
6
9
9
7
7
13
15
14
14
16
16
123
Øye vei
Øy
Øye
111
109
113
10
0
25
50
100 m
Målestokk A3: 1:2 000

Appendix G

MASW-profile location

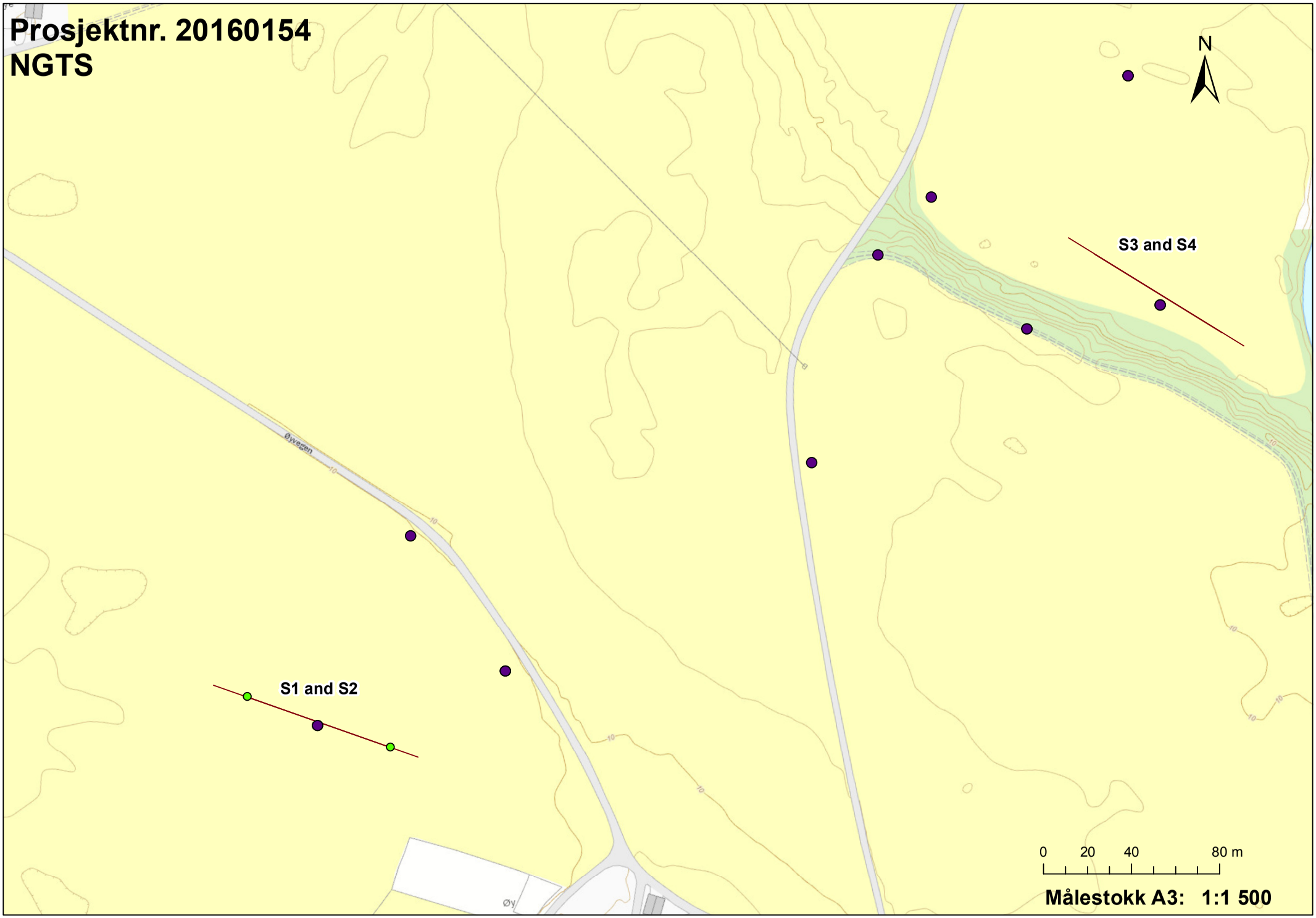
Prosjektnr. 20160154
NGTS
N
S3 and S4
S1 and S2
Øyvegen
0 20 40 80 m
Målestokk A3: 1:1 500

Appendix H

Results CPTU

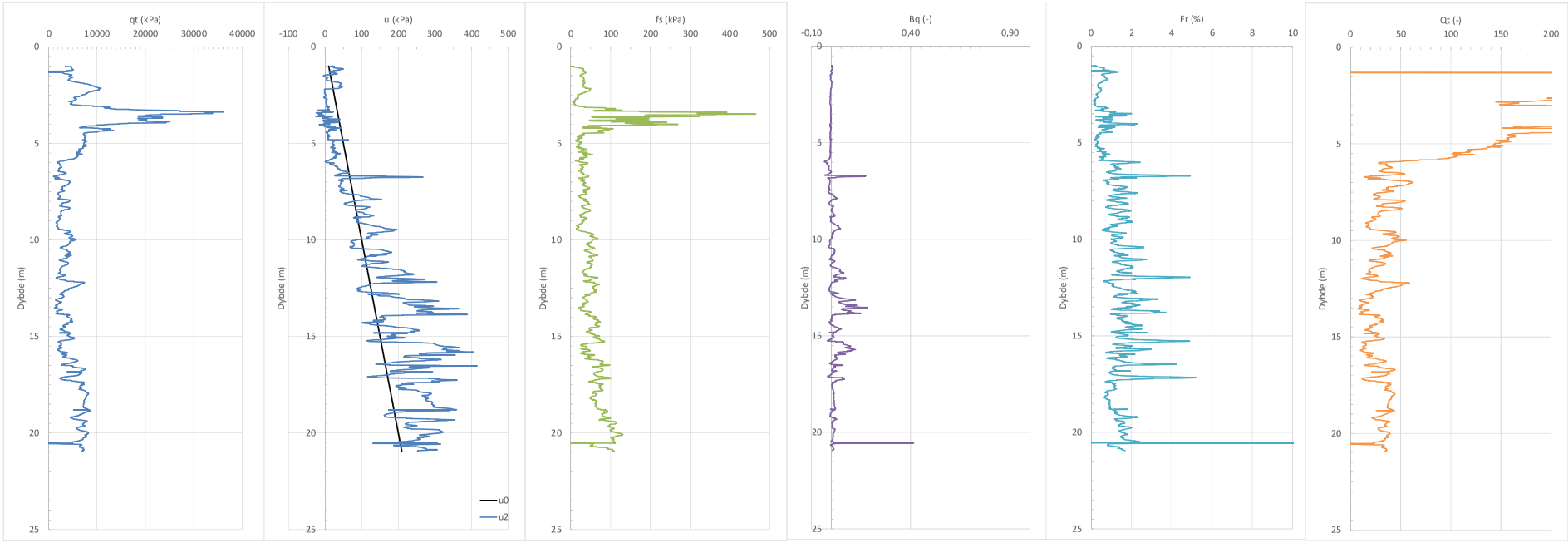

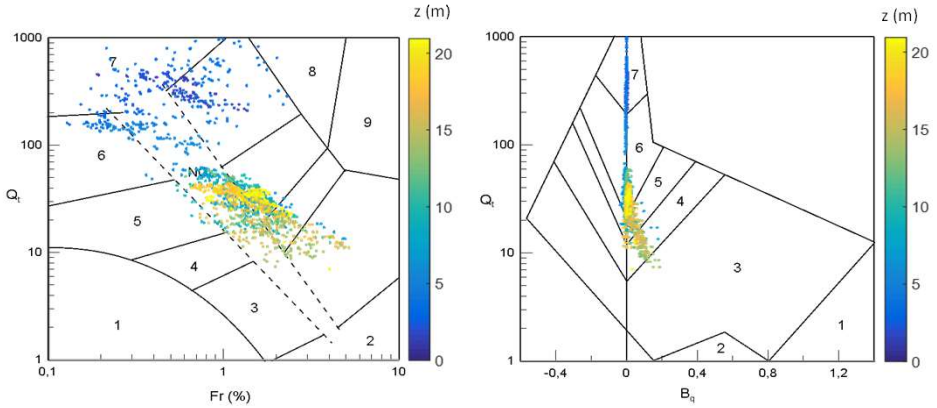

Sone	Jordartsklassifisering
1	Sensitiv, finkornet
2	Organisk jord – leire
3	Leire – siltig leire til leire
4	Siltblandinger – leirig silt til siltig leire
5	Sandblandinger – siltig sand til sandig silt
6	Sand - ren sand til siltig sand
7	Grusig sand til fast sand
8	Veldig stiv sand til leirig sand
9	Veldig stiv, finkornet

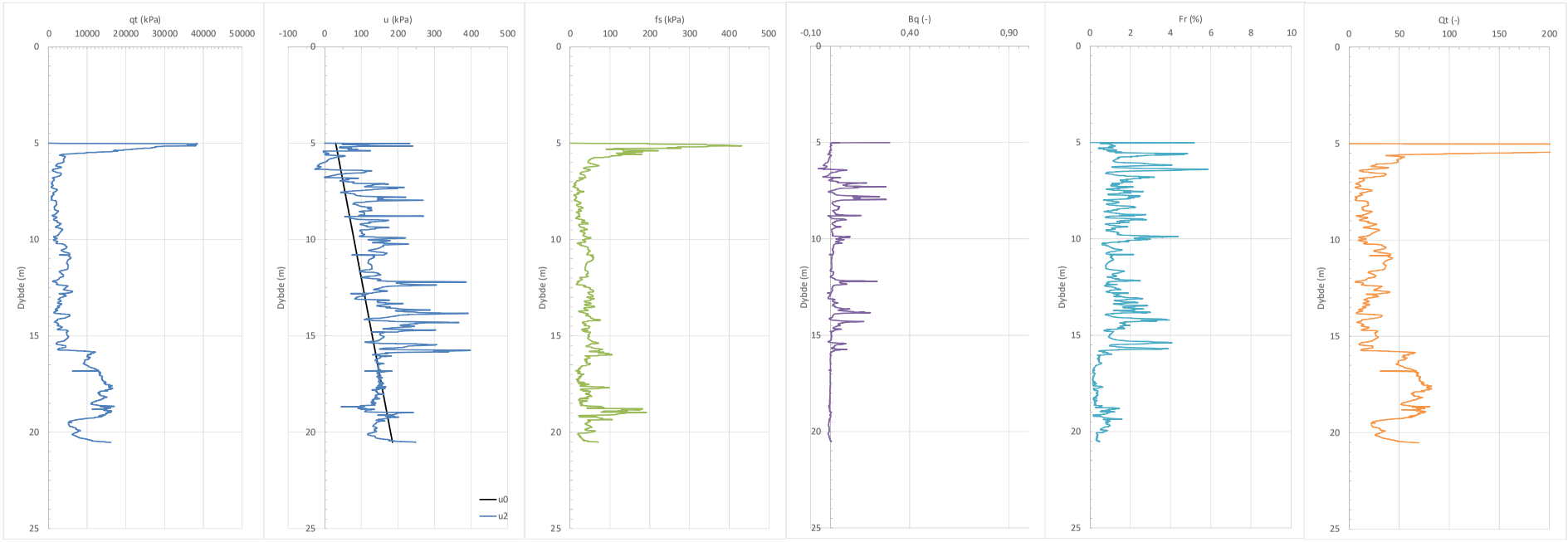

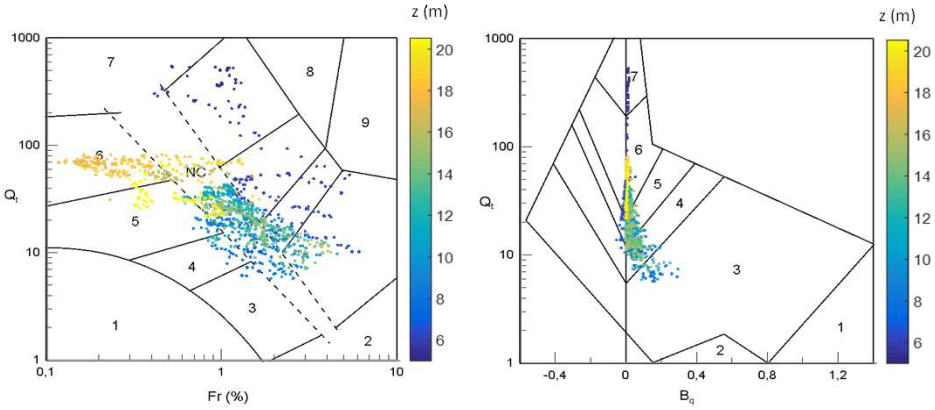

Sone	Jordartsklassifisering
1	Sensitiv, finkornet
2	Organisk jord – leire
3	Leire – siltig leire til leire
4	Siltblandinger – leirig silt til siltig leire
5	Sandblandinger – siltig sand til sandig silt
6	Sand - ren sand til siltig sand
7	Grusig sand til fast sand
8	Veldig stiv sand til leirig sand
9	Veldig stiv, finkornet

Bibliography

Andrus, R. D., Mohanan, N. P., Piratheepan, P., Ellis, B. S., and Holzer, T. L. (2007). Predicting shear-wave velocity from cone penetration resistance. In *Proceedings of the 4th International Conference on Earthquake Geotechnical Engineering, Thessaloniki, Greece*, volume 2528.

Arduino, P. (2000). An introductio to the theory of wave propagation in layer media.

ASTM, S. (2000). Standard practice for description and identification of soils (visual-manual procedure).

ASTM, S. (2007). D422–63 (2007) standard test method for particle-size analysis of soils. *ASTM International, West Conshohocken. doi*, 10:1520.

Atkinson, J. and Sallfors, G. (1991). Experimental determination of soil properties. *Proceedings of the 10th ECSMFE, Florence*, 3:915–956.

Benz, T. (2007). *Small-strain stiffness of soils and its numerical consequences*. Univ. Stuttgart, Inst. f. Geotechnik.

Benz, T., Schwab, R., and Vermeer, P. (2009). Small-strain stiffness in geotechnical analyses. *Bautechnik*, 86(S1):16–27.

Berner, R. A. (1980). *Early diagenesis: A theoretical approach*. Number 1. Princeton University Press.

Blackstock, D. T. (2000). *Fundamentals of physical acoustics*. John Wiley & Sons.

EPA, U. (2016). General crosshole procedures.

GeoScience, H. (1999). Crosshole seismic tomography.

Hardin, B. and Richart Jr, F. (1963). Elastic wave velocities in granular soils. *Journal of Soil Mechanics & Foundations Div*, 89(Proc. Paper 3407).

Idriss, I. and Seed, H. (1970). Soil moduli and damping factors for dynamic response analysis. *Report EERC*, 70(10).

Kramer, S. L. (1996). *Geotechnical earthquake engineering*. Pearson Education India.

Marchetti, S. (1980). In situ tests by flat dilatometer. *Journal of Geotechnical and Geoenvironmental Engineering*, 106(ASCE 15290).

Marchetti, S., Monaco, P., Totani, G., and Marchetti, D. (2008). In situ tests by seismic dilatometer (sdmt). *From research to practice in geotechnical engineering*, 180:292–311.

Mjaavatten, E. (2007). Håndbok fra skog og landskap 03/2007 feltinstruks for jordsmonnkartlegging.

NGU (2016). Løsmassekart.

NS8005 (1990). Geoteknisk prøving - laboratoriemetoder - kornfordelingsanalyse av jordprøver. *93.020 - Jordarbeider. Utgraving. Fundamentering.*

Park, C. B., Miller, R. D., Xia, J., and Ivanov, J. (2007). Multichannel analysis of surface waves (masw)—active and passive methods. *The Leading Edge*, 26(1):60–64.

Rix, G. J. and Stokoe, K. H. (1991). Correlation of initial tangent modulus and cone penetration resistance. In *International Symposium on Calibration Chamber Testing*, pages 351–362. New York: Elsevier Publishing.

Robertson, P. (1990). Soil classification using the cone penetration test. *Canadian Geotechnical Journal*, 27(1):151–158.

Robertson, P. (2009). Interpretation of cone penetration tests-a unified approach. *Canadian Geotechnical Journal*, 46(11):1337–1355.

Robertson, P. K. and Campanella, R. (1983). Interpretation of cone penetration tests. part i: Sand. *Canadian geotechnical journal*, 20(4):718–733.

Robertson, P. K., Campanella, R. G., Gillespie, D., and Rice, A. (1986). Seismic cpt to measure in situ shear wave velocity. *Journal of Geotechnical Engineering*, 112(8):791–803.

Stokoe, K., Darendeli, M., Andrus, R., and Brown, L. (1999). Dynamic soil properties: laboratory, field and correlation studies. In *Proc. 2nd Int. Conf. Earthquake Geotech. Engg*, pages 811–846.

Survey, K. G. (1998). Kansas geological survey.

Tom Lunne, Peter K. Robertson, J. J. P. (1997). *Cone Penetration Testing In Geotechnical Practice*. Blackie Academic & Professional, first edition.

Vegvesen, S. (2005). Vedlegg 1 jordartsklassifisering. *Håndbok 014 Laboratorieundersøkelser*.